J. Fluid Mech. (1990), *vol.* 210, *pp.* 371–414
Printed in Great Britain

Three-dimensional large-eddy motions and fine-scale activity in a plane turbulent wake

By J. A. FERRÉ[1], J. C. MUMFORD[2], A. M. SAVILL[2] AND FRANCESC GIRALT[1]

[1] Departament d'Enginyeria Química i Bioquímica, Divisió VII, Universitat de Barcelona, 43005 Tarragona, Catalunya, Spain

[2] Department of Engineering, University of Cambridge, Trumpington Street, Cambridge CB2 1PZ, UK.

(Received 8 October 1988 and in revised form 3 July 1989)

A pattern recognition technique has been applied to simultaneously sampled multipoint hot-wire anemometry data obtained in the far wake of a circular cylinder. Data from both the streamwise fluctuating velocity field and the temperature field have been analysed employing a computer code that uses a correlation approach to automatically detect and ensemble average flow patterns and patterns for mean-square fluctuations. Statistical tests then allow the significance and contribution to the turbulence intensity of the detected structures to be evaluated. This procedure has been used to infer the three-dimensional topology of the double-roller eddies previously identified in the far-wake region and to relate these to the motions responsible for entrainment. It appears that the two types of motion are not independent, but are linked together, forming parts of horseshoe vortex structures which account for at least 40% of the total turbulence energy. These structures originate near the centre of the flow, may extend across the centreline and typically occur in groups of about three. The resulting picture of the flow dynamics is related to the conclusions drawn from similar data by other workers and a possible regeneration mechanism is presented. The addition to the code of a fine-scale activity indicator, the choice of which is discussed in some detail, has allowed the relationship between these energetic large-scale motions and smaller eddies to be investigated. It seems that the most intense fine-scale activity is associated with the vortical cores of the double-roller eddies. It is shown that this observation is consistent with the concepts of 'isotropy' and 'spotiness' of the dissipative scales. It also suggests that the horseshoe vortices loose energy both to their own secondary instabilities and to smaller scales resulting from the breakup of other highly strained large eddies.

1. Introduction

The wake flow behind a circular cylinder has, for many years, atrracted the attention of researchers in fluid mechanics and turbulence, even though its technological importance has been regarded as far less than that of boundary-layer flows. Perhaps for this reason, contributions to the understanding of turbulence in boundary layers have been substantially different from the insight gained into the structure and dynamics of wake flows. In boundary layers, the success of visualization techniques has made it possible to interpret instantaneous anemometer signals and those obtained by means of some conditional averaging procedure such as the VITA technique, in terms of the structure of the flow.

The comparison of visualization and anemometry has helped to emphasize that turbulence is by nature three-dimensional. The two-dimensionality in the mean field of many flows is just an artifact introduced by measuring time averages or by applying the time-average operator over the Navier–Stokes equations. On the other hand, wakes and other plane free-shear flows have been mainly examined as two-dimensional 'instantaneous' flows, probably as a consequence of the two-dimensional character of the Kármán vortices and of the very strong and even surprising two-dimensional character of the turbulent shear layer. More recently, it has been observed both experimentally and numerically that shear-layer flows develop three-dimensional structures which ride over two-dimensional vortices (Jimenez, Cogollos & Bernal 1985).

The first hypothesis on the three-dimensional large-scale organization of the far-wake flow can be traced back to the work of Townsend (1956) and Grant (1958), who postulated the existence of shear-aligned double-roller eddies in the far wake of a single cylinder ($x/D = 533$, where x is the streamwise coordinate and D is the cylinder diameter). The problem was re-examined by Payne & Lumley (1967) using the orthogonal decomposition procedure to extract the typical eddy velocity patterns from the correlation data of Grant. The results they obtained, however, were not in total accordance with the hypothesis of Grant. It was not until later that the question of the large eddies in fully turbulent plane wakes (Mumford 1983) and also jets (Mumford 1982) was addressed using a new approach based on a pattern recognition computer code designed to extract repetitive trends embedded in the turbulent signals sensed by a set of anemometers. Mumford (1983) obtained ensemble averages of the typical velocity footprints of the double rollers, and also of single-roller eddies, confirming not only the hypothesis of Grant (1958) on shear alignment, but also making estimates of the range of sizes of the single- and double-roller eddies and of their contribution to the turbulence activity.

Using the same kind of pattern recognition approach, Ferré & Giralt (1989*a*) (hereinafter referred as FG1) analysed the large-scale organized motions in a variety of wakes. These were generated behind arrangements of static and rotating cylinders and included the wake of a single cylinder. They also analysed the organized motions of the thermal field in the wake of a heated cylinder (Ferré & Giralt 1989*b*; hereinafter referred as FG2). Comparing the fully developed region of different wakes at $x/D = 140$, as well as the development of a normal wake from $x/D = 10$ to $x/D = 220$, they analysed the evolution of the Kármán vortex street and the development of single- and double-roller eddies (FG1). The typical large-scale organization was recognized to be double-roller eddies, the single rollers which were observed being only double rollers partially sensed by the limited set of anemometers used. Moreover, the existence of such eddies was not limited to the wake of a single cylinder, but all the wakes analysed contained such kinds of structures, which scaled in size with the half-width of the wake and in intensity with the local turbulence intensity values.

Probably the most interesting results were those obtained in the wake of a heated cylinder (FG2). Relaxing the true intermittency criteria and looking for colder (temperature lower than the mean temperature) and hotter (temperature above the mean value) spots, they observed a strong three-dimensional character of the flow. In the vertical plane of the wake, i.e. in the shear plane, the thermal field displayed an organization consisting of temperature fronts. In a horizontal plane located at the position of maximum shear, the temperature spots showed a spanwise and streamwise extension not larger than 1.8 half-width units. The limited extent of the hot spots in

the spanwise coordinate and their shear-aligned character in the vertical plane led to the hypothesis that the double-roller eddies are in fact associated with the large-scale entraining motions of the wake.

The organized motions in the fully developed region of a plane jet (Antonia *et al.* 1986) and of a wake (Browne, Antonia & Bisset 1986) have been analysed recently using a conditional sampling procedure. The triggering signal used to obtain the ensemble averages was based on a true three-dimensional feature of the thermally contaminated flow. The ensemble averages themselves were obtained in the shear plane of the flow, showing only a vertical slice of the three-dimensional organized motions. Despite this restriction, these results are a valuable point of reference for our findings and also for the pattern recognition analysis of the thermally contaminated wake (FG2). A comprehensive comparison between present results and those reported by Browne *et al.* (1986) will be presented later.

This paper deals with a further and deeper analysis of the velocity signals measured in the wake of a single cylinder at $x/D = 140$, with three main objectives. First, the detailed topology of the double rollers is investigated and their sense of rotation and relation to the turbulent/non-turbulent interface established. Secondly, the mechanism of entrainment by engulfing, which should be related to the large-scale motions in the wake, is investigated and its dependence on the velocity fields induced by the double-roller eddies clarified. The final objective is to evaluate the role played by these eddies in the turbulence activity of the wake in two important aspects: their contribution to the turbulence intensities or r.m.s. levels in the wake and the dependence of the fine-scale activity in the wake on the large-scale motions.

In the following sections, a brief description of the experimental set-up will be presented. After this follows a discussion of the analytical and statistical tools, and on the fine-scale indicator function used. The main results are presented in two further sections. The first of these reports results concerning the large-scale organization in the far wake, while the second section deals mainly with the fine-scale activity. The paper concludes with a discussion that attempts to draw a picture of the turbulent activity in the self-preserving region of the wake, relating the large-scale motions to the engulfing process and to the energy cascade process that transfers energy from the mean flow to the dissipative eddies.

2. Experimental equipment

The wake studied was generated in the open-circuit, suction-type wind tunnel of the Department of Chemical Engineering and Biochemistry of the University of Barcelona in Tarragona. The experimental section was 60×60 cm and 3 m long. A set of flow straighteners and filters, and a contraction zone of ratio 9:1 produced a low-turbulence (less than 0.05%) free-stream flow that was continuously controlled from 2 to 20 m/s by a variable-speed fan. All data were obtained at $Re = 9000$, based on the free-stream velocity (7 m/s) and the cylinder diameter (19.3 mm). The data acquisition system was based on a 12-bit A/D converter supported by a PDP 11/60 computer. The voltage signals were offset to zero, amplified and low-pass filtered at 2 kHz before being sampled at 5 kHz per channel. Continuous records of 40 s were digitized, obtaining data files with 200000 samples per channel. After being digitized, the voltage signals were copied onto magnetic tapes and processed on a mainframe computer.

Eight normal-wire constant-temperature anemometers (DISA 55M01/55M10 bridges and 55P11 probes) operated at an overheat ratio of 1.8 were used to sample

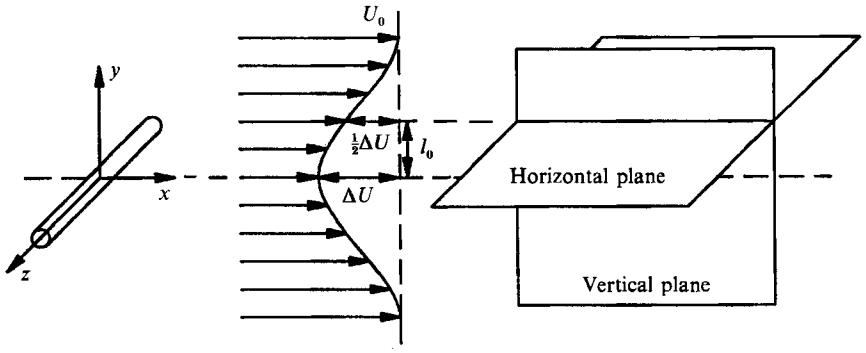

FIGURE 1. Flow configuration and sampling planes.

turbulent u-velocities in the wake. The anemomcters were calibrated assuming a King's law relation

$$E = A + BU^n, \tag{1}$$

where E is the bridge voltage and U the streamwise velocity. Constants A, B and n were determined from velocities measured with a Pitot tube and a differential-pressure cell, in the empty working section of the wind tunnel, and from the corresponding anemometer voltages obtained by A/D conversion.

The data acquisition in the wake was performed at $x/D = 140$ in two orthogonal planes, as shown in figure 1. The spacing between anemometers was selected to be 0.6 times the half-width of the wake l_0, defined as the distance between the maximum velocity defect and the half-velocity defect positions. For the current experimental conditions $l_0 = 64$ mm, approximately. With this arrangement the anemometers covered the full velocity defect in the vertical plane, and an equivalent length in the horizontal one. In the horizontal plane, the anemometers were placed at the half-width position which coincides, approximately, with the maximum Reynolds stress position. Further details of the experimental set-up can be found in FG1.

3. Analysis procedure

The procedure used to analyse the data files obtained in the wake was based on the pattern recognition computer code described in FG1. In short, the pattern recognition approach applied is a signal-processing-oriented technique, designed to extract repetitive trends embedded in single or multi-channel stochastic signals. The method is flow independent, but the significance of results strongly depends upon the spatial distribution of the sensors. Use of Taylor's hypothesis of frozen turbulence has to be made to interpret the time footprints of the organized motions as spatial distributions. However, it is never explicitly necessary to convert the time coordinate into an spatial one, neither is there a need to choose a convection velocity. The only approximation relies on accepting that the large-eddy motions do not change significantly while crossing the set of anemometers. This is an hypothesis that seems to be particularly well suited for the far wake, a flow with a low velocity defect and turbulence intensity level, but with a relatively high absolute convection velocity.

3.1. *Data normalization, ensemble averages and statistical tests*

After several individual realizations of a repetitive trend are detected, they are added together to form an ensemble average. Ensemble averaging is not just a procedure to eliminate the random effects of the finer scales of the turbulence over the organized motions, but is a key step from a statistical point of view. In fact, when a family of characteristic footprints is supposedly detected, the question that arises is whether they are really organized, and thus non-random, or whether they are no more than the consequence of the randomness of turbulent signals which can contain many different 'typical' footprints, identifiable perhaps by visual inspection, but not representative of any kind of organized motion. Ensemble averaging, however, allows one to compute significance levels for the ensemble-averaged quantities which will give a measure of the degree of similitude or difference with respect to the conventional mean values, as explained in FG1.

The u-velocity corresponding to each anemometer was centred to zero, by subtracting its mean value, and normalized by dividing by its r.m.s. values. While this seems to be the appropriate procedure when the anemometers are placed in the horizontal plane, spanning along the homogeneous coordinate of the flow, in the vertical plane it has to be taken into account that this procedure gives more importance to the topological features of the organized motions at the expense of enhancing the velocity signals in the outer wake anemometers. Significance levels can be computed irrespective of whether the data are centred to zero or not. However, in order to clearly separate the effects of the mean flow from those of the organized motion, it is convenient to give a zero mean value to the data in such a way that non-zero-mean ensemble-averaged values are easily identified as 'organized motions', while zero-mean averaged values correspond to the conventional mean values.

The m_x data windows of normalized velocities $U(i,j)$ that are recognized to contain the footprints of some organized motion, are summed to obtain the ensemble average $\langle U\rangle(k,l)$. Further details on how to obtain the velocity footprints of the organized motions, as well as the statistical test applied to compute the probability of obtaining such patterns only by chance can be found in FG1. In order to further investigate the characteristics of the flow, ensemble averages of the squared fluctuating velocities have been also obtained as

$$\langle U^2\rangle(k,l) = \frac{1}{m_x}\sum_{1}^{m_x} U^2(I(m)+k, J(m)+l). \tag{2}$$

$I(m)$ and $J(m)$, $m = 1, 2, \ldots, m_x$ are the vectors indicating the positions where the data frames to be averaged are located within the $U(i,j)$ matrix.

The values $\langle U^2\rangle(k,l)$ could be checked for statistical significance using the same procedure as for ensemble-averaged velocities, if they were normalized using their own mean and variance values. However, if the data are considered to be approximately normally distributed, then the sum of squares for a single point (k_0, l_0), denoted by s_0^2,

$$s_0^2 = m_x\langle U^2\rangle(k_0,l_0) = \sum_{1}^{m_x} U^2(I(m)+k_0, J(m)+l_0), \tag{3}$$

is well described by a Chi-square distribution with m_x degrees of freedom. In addition, for $m_x > 30$ a standard normal approximation to the Chi-square distribution can be obtained if the sum of squares is transformed according to

$$z_0 = (2s_0^2)^{\frac{1}{2}} - (2m_x - 1)^{\frac{1}{2}} \tag{4}$$

This standard normal variable z_0 can be rewritten as

$$z_0 = (2m_x - 1)^{\frac{1}{2}}[(s_0^2/m_x)^{\frac{1}{2}} - 1] \tag{5}$$

after approximating $[2m_x/(2m_x-1)]^{\frac{1}{2}} = 1$. By reordering the terms and going back to the $\langle U^2 \rangle (k,l)$ notation, (5) reduces to

$$z_0 = (2m_x - 1)^{\frac{1}{2}}[\langle U^2 \rangle^{\frac{1}{2}}(k_0, l_0) - 1]. \tag{6}$$

The main advantage of presenting the data this way is that by plotting the data as $\langle U^2 \rangle^{\frac{1}{2}}(k,l) - 1$, only points departing from the conventional sum of squares exhibit non-zero values, while the points with a sum of squares near the values that could be expected for a random selection of data windows exhibit near-zero values. Therefore, only the organized or coherent part of the information contained in the sum of squares is displayed, avoiding any mix of the contributions from the conventional time means with those from the fluctuating, but organized, velocity field.

The significance of the non-zero values of the sum of squares can be assessed using the same procedure that was employed for the mean values, now taking as limits of integration $\pm z_0$. The significance level obtained not only measures, in a probabilistic sense, how different from the conventional values those obtained are, but also corresponds to the significance level that should be used to reject the null hypothesis $H_0 : \langle U^2 \rangle^{\frac{1}{2}}(k_0, l_0) = 1$, against the alternative hypothesis $H_1 : \langle U^2 \rangle^{\frac{1}{2}}(k_0, l_0) \neq 1$ in a two-sided test. The fluctuating velocities $U(i,j)$ averaged to obtain $\langle U^2 \rangle (k,l)$ are the same quantities used to obtain the r.m.s. values associated to each anemometer, apart from a scale factor. They measure departures from the time-mean velocities. As a consequence, the ensemble-averaged sum of squares of the fluctuating velocities can be interpreted as a map of the contribution by the organized motions to the r.m.s. values sensed by each anemometer. Positive values of $\langle U^2 \rangle^{\frac{1}{2}}(k,l) - 1$ will show the regions contributing more to the r.m.s. levels, while negative values will mark those regions showing a deficit in its contribution to the r.m.s.

If the square of the ensemble-averaged values is subtracted from the ensemble average of squares, $\langle U^2 \rangle (k,l) - \langle U \rangle^2 (k,l)$, the new variable obtained can still be interpreted as a sum of squares of fluctuating velocities. However, these new fluctuating velocities are not deviations from the time-mean velocities, but from the velocities of the ensemble-averaged pattern, in such a way that if all the patterns averaged were identical, then

$$\langle U^2 \rangle (k,l) - \langle U \rangle^2 (k,l) = 0. \tag{7}$$

This new quantity measures the variance of the family of averaged patterns with respect to its mean value $\langle U \rangle (k,l)$. Since this is a sum of squares, the data can be presented as before, and significance levels can also be computed in the same way. The only difference is that now the number of degrees of freedom of the chi-square distribution is $m_x - 1$, because a computed mean value is used instead of the 'true' mean value of the population. So then, the data will be plotted as $[\langle U^2 \rangle (k,l) - \langle U \rangle^2 (k,l)]^{\frac{1}{2}} - 1$, which is proportional to the standard normal variable

$$z_0 = (2m_x - 3)^{\frac{1}{2}}[(\langle U^2 \rangle (k_0, l_0) - \langle U \rangle^2 (k,l))^{\frac{1}{2}} - 1]. \tag{8}$$

The significance level obtained for z_0 also corresponds to the critical value of a two-sided test with the null hypothesis $H_0 : [\langle U^2 \rangle (k_0, l_0) - \langle U \rangle^2 (k_0, l_0)]^{\frac{1}{2}} = 1$ and the alternative hypothesis $H_1 : [\langle U^2 \rangle (k_0, l_0) - \langle U \rangle^2 (k_0, l_0)]^{\frac{1}{2}} \neq 1$. This test makes a comparison between the observed fluctuations of the different patterns with respect to its

mean value and the fluctuations of the raw data. As a consequence, negative values of $\langle U^2\rangle - \langle U\rangle^2$ will mark those parts of the ensemble averages that show less variation among the individual patterns than the raw data shows, while positive values will indicate that the dissimilarities among the individual realizations used to form the ensemble average are even greater than those that could be expected for a data point with such an r.m.s. value. In other words, if the selection of data windows were done at random, then a zero ensemble-averaged pattern would be obtained, $\langle U\rangle(k,l) = 0$, and the expected value of $\langle U^2\rangle - \langle U\rangle^2$ would be simply unity, i.e. the r.m.s. value of the data.

Sometimes $\langle U^2\rangle - \langle U\rangle^2$ has been interpreted has an indicator function of the fine-scale activity linked to the organized motions. This would be true if the only differences among all the patterns in one family were the consequence of secondary instabilities developed over the single basic coherent structure. However, dissimilarities among individuals in one family can also be attributed to different size, intensity, orientation and even to misalignment of the individual data windows averaged, as a result of the detection scheme used. Therefore, only when the typical footprints of the organized motions do not exhibit a range of sizes and intensities, can $\langle U^2\rangle - \langle U\rangle^2$ be interpreted as a fine-scale activity indicator function. As this is not the case for the far wake, where a range of organized motions can be detected (Savill 1979; Mumford 1983), the activity in the fine scale has been examined using a procedure independent of the size and intensity of the footprints of the large eddies.

3.2. *Contribution of the large eddies to turbulence activity*

The ensemble averages $\langle U^2\rangle$ can be used to analyse the contribution from different parts of some organized motion to the r.m.s. values, as discussed in §3.1. However, it would be interesting to evaluate the neat effect of the organized motions on the turbulent activity of the wake or, stated in other terms, it would be useful to know how different the wake flow would be if a particular kind of large-scale motion were suppressed. As the only information to hand is the u-velocities, it seems adequate to answer this question by evaluating the contribution to the r.m.s. of each anemometer by the large eddies. Once a family of repetitive trends is detected in a data file, this is re-examined to compute new statistics for a set of modified velocities from which the effect of the large-scale ordered motions have been removed, by subtracting the ensemble-averaged pattern $\langle U\rangle(k,l)$ from the data file in all the data windows that contributed to the ensemble average.

3.3. *A fine-scale activity indicator function*

In order to investigate the activity of the finer scales in the flow and its relation to the large-scale motions, a fine-scale-activity indicator function is needed. This indicator function should be an 'instantaneous' signal that associates some degree of activity in the fine scale to the velocity signals that are used in the pattern recognition analysis. Some of the previous experimental studies related to the fine-scale intermittency of turbulence have been carried out using an approach based on band-pass filtering the velocity signals (see Sreenivasan 1985 and related references for example). However it seems rather risky or arbitrary to select some typical frequency and band-width as representative of the fine-scale activity in the wake.

For isotropic turbulence, the dissipation term in the transport equation for the turbulent kinetic energy reduces to a term proportional to the time average of the square of the first derivative of the u-velocity with respect to the x-coordinate, which in turn can be related to the first time derivative of the velocity signals. This suggests

that a fine-scale indicator function could be based on the first derivatives of the signal. However, for non-isotropic flows, the evaluation of dissipation under the aforementioned assumptions has been shown to be a crude approximation (Müller & Mu 1987). In addition, there are doubts concerning the ability of the first derivatives to display true 'instantaneous' properties of the turbulent flow. Any well-designed fine-scale-activity indicator function should yield zero values for the non-turbulent zones of the flow and positive values for the turbulent zones. The first derivatives of the velocities are known to be a poor indicator of intermittency (Muck 1980). It was therefore decided to use the second time derivatives of the velocity signals as the basis for the fine-scale-activity indicator.

There are two main problems in using the raw second derivatives to detect the finer scales of the turbulence. The first is that the second derivatives are doubled-sided signals, with positive and negative values, when one wants a positive signal. The second is that the frequency content of the second-derivative signals is shifted towards the high frequencies in the spectrum, producing an 'artificially' enhanced decorrelation between the velocity signals and their second derivatives. A way to overcome both of these drawbacks is to further process the second derivatives to obtain their envelope. This last step allows one to convert the double-sided signal into a positive definite signal in a natural way, while, simultaneously, the spectrum of the signal is shifted back to lower frequencies. The envelope of the second time derivatives of the velocity signals was therefore used as the fine-scale-activity indicator function.

The envelope of a band-limited signal is defined as the modulus of a complex signal, called the pre-envelope, whose real part is the original data and the imaginary part is the Hilbert transform of the raw signal. If $s(t)$ is the band-limited signal, and $r(t)$ is its real-valued Hilbert transform, then the pre-envelope $p(t)$ can be written as

$$p(t) = s(t) + \mathrm{i}\, r(t). \tag{9}$$

The Hilbert transform of $s(t)$ is more appropriately defined by relating its Fourier transform to that of the raw data. If F is the Fourier transform operator, and $S(f)$ is the Fourier transform of $s(t)$, defined by

$$\mathrm{F}[s(t)] = S(f) = \int_{-\infty}^{+\infty} s(t) \exp(-\mathrm{i}2\pi f t)\, \mathrm{d}t, \tag{10}$$

then the Fourier transform of $r(t)$, can be related to $S(f)$ by

$$\mathrm{F}[r(t)] = \begin{cases} -\mathrm{i}S(f) & \text{if } f > 0 \\ 0 & \text{if } f = 0 \\ \mathrm{i}S(f) & \text{if } f < 0. \end{cases} \tag{11}$$

Once the pre-envelope of a signal is obtained, its envelope $e(t)$ is computed as

$$e(t) = [s(t)^2 + r(t)^2]^{\frac{1}{2}}. \tag{12}$$

The derivatives of a signal can also be computed spectrally with maximum accuracy. If $u(t)$ is the function that has to be derived and $U(f)$ is its Fourier transform, then the Fourier transform of the derivatives of $u(t)$ can be obtained as

$$\mathrm{F}\left[\frac{\mathrm{d}^n u(t)}{\mathrm{d}t^n}\right] = U(f)\,(\mathrm{i}2\pi f)^n. \tag{13}$$

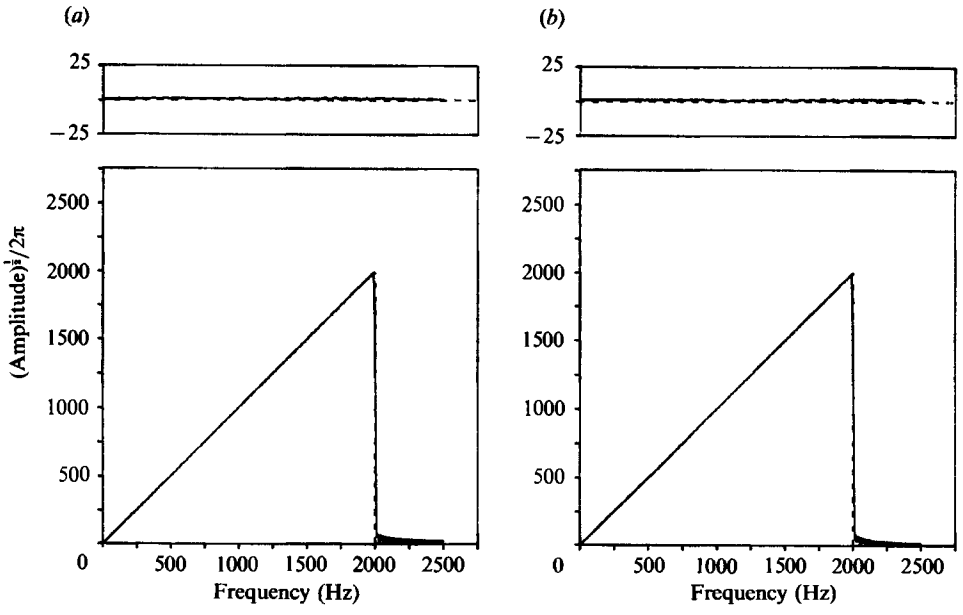

FIGURE 2. Characteristics of the filters used to obtain (*a*) the real and (*b*) the imaginary parts of the pre-envelope of the time second derivatives of the signals.

In particular, if $u(t)$ is a turbulent velocity, $s(t)$ is its second derivative and $U(f)$ and $S(f)$ are their respective Fourier transforms, then $S(f) = -U(f)(2\pi f)^2$.

Therefore, it is possible to implement in one step both the computation of the second derivatives and of the real and imaginary parts of the pre-envelope, from which the envelope can be obtained. The development of a computational version of this procedure required the design of two constant-phase-lag digital filters, which were implemented as symmetric finite impulse response filters. The filter design was achieved by a windowing technique using a Hamming window (Chen 1979). Although this requires the use of longer filters to maintain specifications when compared to other design techniques, the virtual lack of restrictions on the length of the filter due to the nature of the data (200000 samples of continuous data per channel) made it possible to obtain high-quality filters, virtually free of the ripples caused by the truncation effect.

The envelope of a signal is defined assuming that the signal is band-limited. It might seem therefore rather surprising that an envelope is obtained in this case for the continuous-spectrum turbulent velocities. However, it should be recognized that the voltage signals have been low-pass filtered at 2 kHz before being sampled at 5 kHz per channel, more than two times the cut-off frequency of the filter. Hence the raw velocity signals are actually band-limited. At the same time the procedure of obtaining second derivatives acts as a kind of filter by enhancing the components at higher frequencies by multiplying the Fourier transform of the data by the square of the frequency. In order to avoid this last effect producing aliasing in the envelope, due to leakage of the analogue filter resulting from its transition band and finite attenuation, the digital filters designed to obtain the real and imaginary parts of the pre-envelope incorporated also a low-pass filter with a cutoff frequency of 2 kHz.

The characteristics of the filters used are presented in figure 2. Figure 2(*a*) shows the real part of the truncated filter used to compute the second derivatives; above

it is also plotted the imaginary part which should be zero. Figure 2(*b*) shows the imaginary part of the filter that implements in one step the Hilbert transform and the second derivatives; above this is also plotted the real part that is again expected to be zero. In both cases the characteristics of the ideal filter are plotted as a dotted line.

Significance levels for the ensemble-averaged envelope of the second derivatives have been computed based on the use of the Central Limit Theorem to obtain the sampling distribution of the averages. If $E(i,j)$, $i = 1,2,\ldots i_x$, $j = 1,2\ldots j_x$ is the envelope of the second derivatives at the point (i,j), then a normalized envelope with zero mean and unit variance $E_n(i,j)$ has been obtained as

$$E_n(i,j) = \frac{E(i,j) - \bar{E}(i)}{E_{\mathrm{RMS}}(i)}, \tag{14}$$

where $\bar{E}(i)$ and $E_{\mathrm{RMS}}(i)$ are the mean and r.m.s. values of the envelope for each anemometer. Irrespective of the parent distribution of $E_n(i,j)$, the sampling distribution of its ensemble average will be a normal p.d.f. with zero mean and variance $1/m_x$ for $m_x > 30$. Once again, with data presented in this way, values of the fine-scale activity indicator function which do not depart from the conventional mean value will appear as zero values. Non-zero values will be obtained only for positive or negative deviations, showing an excess or defect of fine-scale activity with respect to the mean activity of the fine scales in the wake.

4. Three-dimensional motions in the far wake

Using a pattern recognition technique, Mumford (1983) analysed the large-scale motions in the far wake of a single cylinder using the data of Savill (1979). He observed that the typical large-scale structures were the single- and the double-roller eddies described by Grant (1958) and Townsend (1976). However, there were doubts on the identity of the single-roller eddies because the velocity patterns observed could also be produced by misaligned double rollers sensed partially by the set of anemometers. Evidence that the double rollers represent the typical organized eddies in wake flows was obtained by FG1 using a simultaneous double-classification pattern recognitioin technique. They observed that it was not possible to obtain single-roller velocity footprints without evidence of double-roller organization in the wake of a single cylinder and in those generated behind several arrangements of static/rotating cylinders of equal and unequal diameters. At the same time the size and intensity of the large-scale motions in the far wake were observed to scale with the half-width and the r.m.s. values of the turbulent u-velocities, respectively, at several downstream positions for the normal wake beyond $x/D = 60$ and at $x/D = 140$ for other wakes. These findings suggested that the far wake is a flow evolving independently of initial conditions and that it could be considered self-similar not only in the mean flow sense but also in its instantaneous large-scale eddies.

The results presented in this section correspond to a deeper analysis of the detailed structural characteristics of the double-roller eddies and of their relation to the entrainment process in the far wake. The analysis is performed by making use of the information provided by the ensemble-averaged velocities as well as that contained in the ensemble averages of the squared velocities, $\langle U^2 \rangle$ and $\langle U^2 \rangle - \langle U \rangle^2$. The ensemble averages are plotted as maps of the averaged quantities with oriented

arrowheads proportional to their magnitude and showing their sign (positive values produce right-oriented arrowheads). Isolevel contours at $\pm 75\%$, $\pm 50\%$, $\pm 25\%$ and $\pm 10\%$ of the peak signal value have been added to aid recognition of the spatial organization in the ensemble averages. The vertical axis is the spatial coordinate plotted in half-width units. The horizontal axis is the temporal coordinate plotted also in half-width units after converting the time displacements into spatial ones by using a convection velocity equal to the mean velocity of the set of anemometers. Note that this mean velocity is used only to convert time into space and that local time-mean velocities are used to centre to zero the instantaneous signals before the flow is analysed. The timescale is increasing from right to left in such a way that the window of ensemble-averaged flow is observed moving from left to right, the anemometers being placed along the vertical axis on the right.

To compare the results reported here with those in FG1 and FG2 it has to be noted that in both references the time axis of all maps is plotted increasing towards the right, so that the data windows in FG1 and FG2 are observed flowing from the right to the left. This does not affect the interpretation of the results of FG1 in the horizontal plane because both positive and negative correlated double rollers were averaged. However, in the case of the vertical plane in FG1 and FG2, and in the horizontal plane in the thermally contaminated wake of FG2 it has to be taken into account appropriately.

4.1. *Sense of rotation of the double roller*

The first step in analysing the details of the large-eddy organization of the wake was an attempt to determine the sense of rotation of the double-roller eddies. In principle there seemed to be no reason for any preferred rotating sense to exist, because a double organization of counter-rotating eddies with vorticity of different sign in each of them would always produce a zero mean vorticity balance in any horizontal slice of the flow. The problem was to discern which of the two configurations shown in figures 3(*a*) and 4(*a*) was the typical one, or whether both coexisted in the wake.

The analysis of the data in the horizontal plane at the maximum shear stress position is presented in figures 3(*b*) and 4(*b*), respectively. These organized motions were detected with a significance level of 1.7% and 6.8% and the fraction of flow represented was 46% and 40%, respectively. However the analysis of the ensemble averages of the squared fluctuating velocities, $\langle U^2 \rangle$ and $\langle U^2 \rangle - \langle U \rangle^2$, revealed that the two ensembles were really different. First, the averaged $\langle U^2 \rangle$ patterns of figures 3(*c*) and 4(*c*) suggested that the two types of large eddies could be made of the same basic 'building block', because the positive contribution to the r.m.s. appeared to be always associated with the negative velocity lobes irrespective of the relative position they had in the averaged pattern. Therefore it seemed possible that one was simply a misaligned version of the other, true typical organized structure. Secondly, the fluctuation of the family of patterns over its ensemble average, that is $\langle U^2 \rangle - \langle U \rangle^2$, as presented in figures 3(*d*) and 4(*d*), shows clearly that the double roller with backflow in the centre is the one that allows the best alignment. It has to be taken into account that these data are presented in such a way that near-zero values mean near-conventional r.m.s. values. Therefore negative values in figure 3(*d*), which extend over nearly the whole data window examined instead of over a smaller region as in 4(*d*), mean that most of the individual realizations are more similar when aligned with backflow in the centre. The peak values of figures 3(*d*) and 4(*d*) seem to contradict such interpretation. It should be noted, however, that a

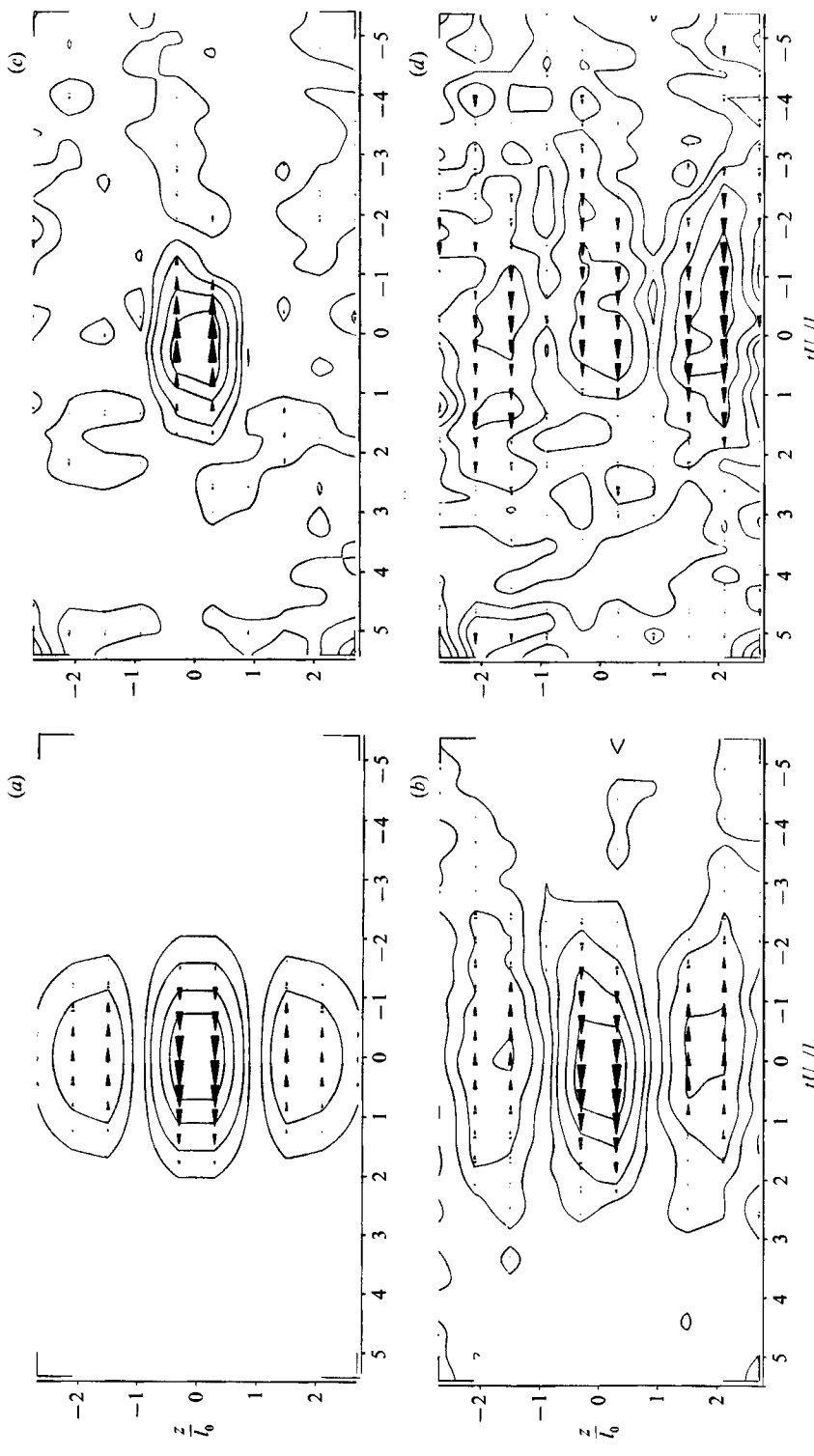

FIGURE 3. Double-roller eddies with central negative velocities: (*a*) template, (*b*) ensemble average, (*c*) $\langle U^2 \rangle$ ensemble average. (*d*) $\langle U^2 \rangle - \langle U \rangle^2$ ensemble average.

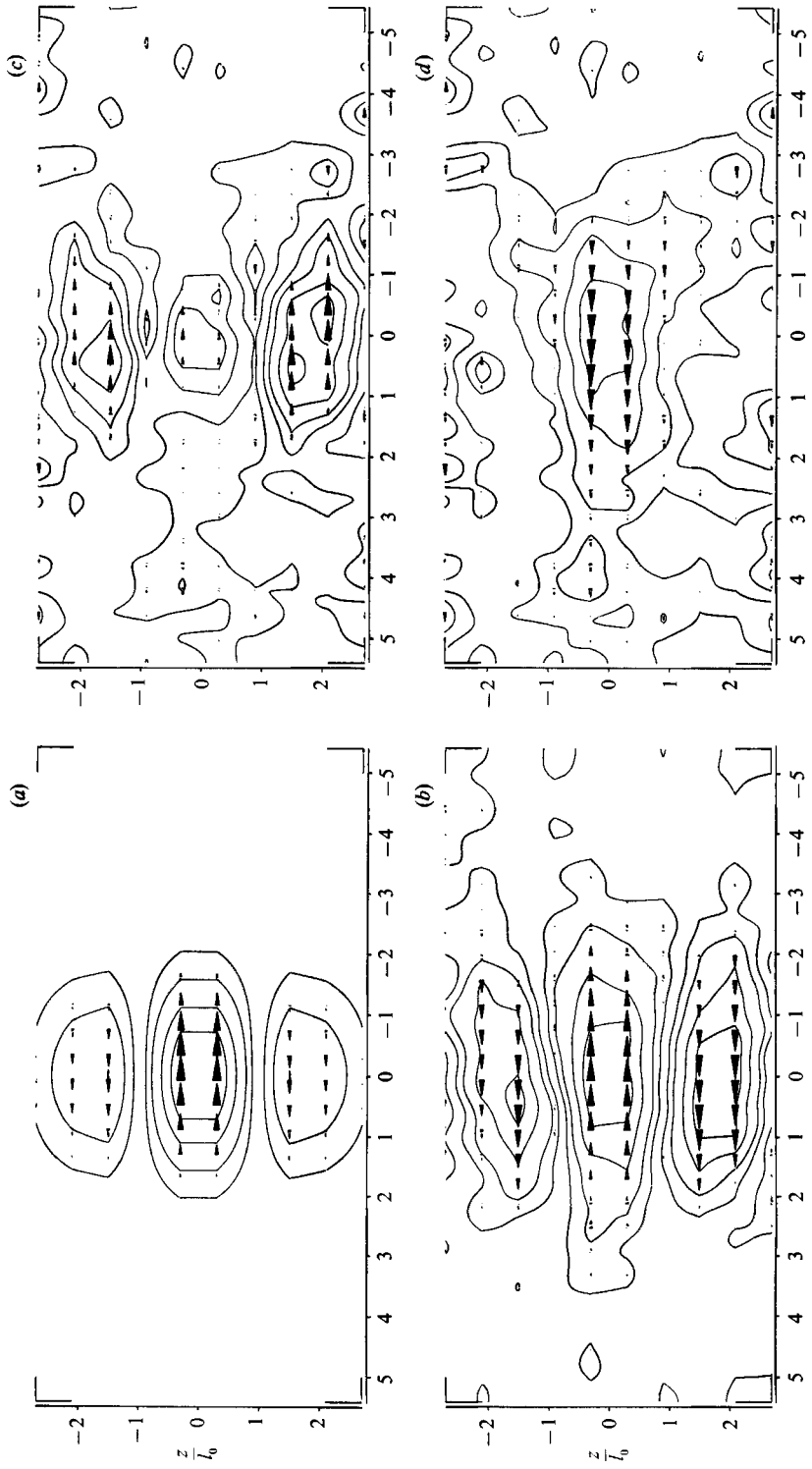

FIGURE 4. Double-roller eddies with central positive velocities: (*a*) template, (*b*) ensemble average, (*c*) $\langle U^2\rangle$ ensemble average, (*d*) $\langle U^2\rangle - \langle U\rangle^2$ ensemble average.

higher absolute peak value is attained in figure 4(*d*) because only the central part of the structure is forced to be aligned, while complete alignment is imposed when obtaining figure 3(*d*).

The peak value of the ensemble in figure 3(*b*) is higher than in figure 4(*b*) by 25%. This fact, together with the previous observation, led to the conclusion that the double-roller eddies with backflow in the centre can explain more of the variability of the raw data by the averaged pattern, and that less 'turbulence' is left to the randomness of the finer scales. If it is assumed that the double-roller eddy with backflow in the centre is the only type of organized motion present in the flow, then one could speculate that they could often occur with a spanwise periodicity because the fraction of flow occupied by the type of structures depicted in figure 3(*b*) is nearly the same as the one for the 4(*b*)-type structures. Such an assumption cannot be checked with present data because the span of the set of anemometers is barely the width of one double-roller eddy. Also, an ensemble average similar to that in figure 4(*b*) could be obtained from data containing only randomly distributed 3(*b*)-type structures, because not only time displacements but also transverse alignment is allowed in the pattern searching procedure.

Another feature of the $\langle U^2 \rangle$ averages (see figures 3*c* and 4*c*) is that the negative u-velocity fluctuations contribute more to the r.m.s. intensities than the positive ones. The latter show again a contribution near to zero because the $\langle U^2 \rangle$ ensemble averages are plotted in such a way that only excess or defect contributions with respect to the conventional r.m.s. values display deviations from zero. This would seem rather abnormal unless we take into account the typical shape and intensity of the 'model' double-roller eddies. The initial templates used by the pattern recognition algorithms have been obtained by simulating the passage of a double roller over the set of anemometers. The velocity patterns of the double rollers are derived from a stream-function model (FG1) which ensures that the relative intensities of the positive and negative velocities are well defined. Therefore, only the double-roller model of figure 3(*a*), with backflow in the centre and with a higher intensity for the negative fluctuations, can be consistent with a large-scale motion that always displays a higher contribution to the r.m.s. values from negative fluctuations.

4.2. *The double-roller eddies and the turbulent/non-turbulent interface*

The analysis of the temperature signals in the far wake of a heated cylinder (FG2) confirmed the strong three-dimensional character of the far wake that might be expected from the existence of double rollers in the flow, but also displayed the typical organization of the entraining motions. A question that remained partially unanswered during the comparison of the results obtained in the normal wake and in the heated wake (see FG2 and FG1) was the relation between the entraining motions and the double-roller eddies.

The pattern recognition analysis of the temperature signals in the horizontal plane revealed a very important feature (FG2). This was that the typical organization of the thermal field was always linked to temperature fronts, mainly sharp hot-to-cold fronts, but also cold-to-hot slopes. These fronts were strongly three-dimensional, with a typical spanwise extent slightly less than approximately two times the half-width of the wake. As velocity and temperature are always negatively correlated in the wake, presenting an extremum near the maximum shear stress position (Fabris 1979), an attempt was made to detect the velocity patterns of the temperature fronts. This was done by checking whether the u-velocity field contained any

organization associated with fast-to-slow (cold-to-hot) and with slow-to-fast (hot-to-cold) velocity gradients. These two velocity patterns are presented in figures 5(*a*) and 6(*a*). The results obtained are presented in figures 5(*b*) and 6(*b*), respectively. For both cases the u-velocity patterns associated with the velocity fronts reveal the typical footprints of the double-roller eddies that had been previously detected. Furthermore, it appears that despite the fact that the initial template contains the same level of positive and negative velocities, the negative velocity fluctuations are those that clearly generate the two additional lobes of positive fluctuations which make the typical velocity footprint of the double roller as observed in figure 3(*b*). Weak negative velocity fluctuations are also triggered by the positive lobes; however, this fact can be easily understood by taking into account the misalignment problem just discussed in the previous section. As a consequence, the double-roller eddies of the wake appear to be definitely characterized by backflow in the centre and also strongly linked to the turbulent/non-turbulent interface (hot-to-cold and cold-to-hot temperature gradients).

The ensemble averages of $\langle U^2 \rangle$ and $\langle U^2 \rangle - \langle U \rangle^2$ are presented in figures 5(*c*) and 6(*c*), and 5(*d*) and 6(*d*), respectively. No new information is displayed that was not observed previously in figures 3 and 4. In short, the maximum contribution to the r.m.s. comes from the central negative velocity fluctuations, and the fluctuations over the ensemble-averaged pattern are for both cases less than the typical r.m.s. values of the data. The scatter observed in figures 5(*c*), 5(*d*), 6(*c*) and 6(*d*) is closely related to the low significance level of the lowest isolevel contours of the plots (see table 1, below). Apart from this effect, there is a clear difference in the 'neatness' of the averaged patterns of figures 5(*b*) and 6(*b*). Although this will be discussed later, the suggestion is advanced that this is produced by the differences that can be observed between the trailing and leading edges of the double-roller eddies, which in turn are influenced by the organization of the tops of the double-roller eddies.

One of the first questions that arise when comparing figure 3(*b*) with figures 5(*b*) and 6(*b*) is why, when the pattern recognition procedure is asked to take ensemble averages of the double roller velocity footprints, the velocity gradients (slow-to-fast or fast-to-slow) associated with the central lobe of negative velocities do not appear. The answer is the same as that given to explain the sometimes weak, sometimes strong, evidence for hot-to-cold and cold-to-hot fronts in the temperature signals (FG2). In short, this will be the case unless organization always occurs at a constant spacing, because the parts of the ordered motion that are not in the centre of the ensemble averaging window are smeared out.

Before the streamwise velocity gradients could be definitely linked to the temperature fronts observed in the thermally contaminated wake (FG2) a very important question remained to be answered. The link between both kinds of gradient has been justified on the basis of the velocity–temperature correlations in the wake (Fabris 1979). However, the spanwise extents of the velocity gradients plotted in figures 5(*b*) and 6(*b*) do not match the extents of the temperature fronts, which were observed to involve four anemometers instead of only two. The interpretation of this apparent mismatch can be obtained from figures 7 and 8. Figure 7(*a*) shows the streamlines of a 'model' double-roller eddy, while figure 7(*b*) shows the corresponding velocity footprints, which are similar to those already presented in figures 3, 5 and 6. Figure 7(*c*) includes the vorticity field associated with this model eddy, contoured at levels $\pm 75\%$, $\pm 50\%$, $\pm 25\%$ and $\pm 10\%$. The two additional sign-inverted lobes of vorticity appearing in figure 7(*c*) are typical of the Gaussian-damped stream-function model, but do not play any role in the present

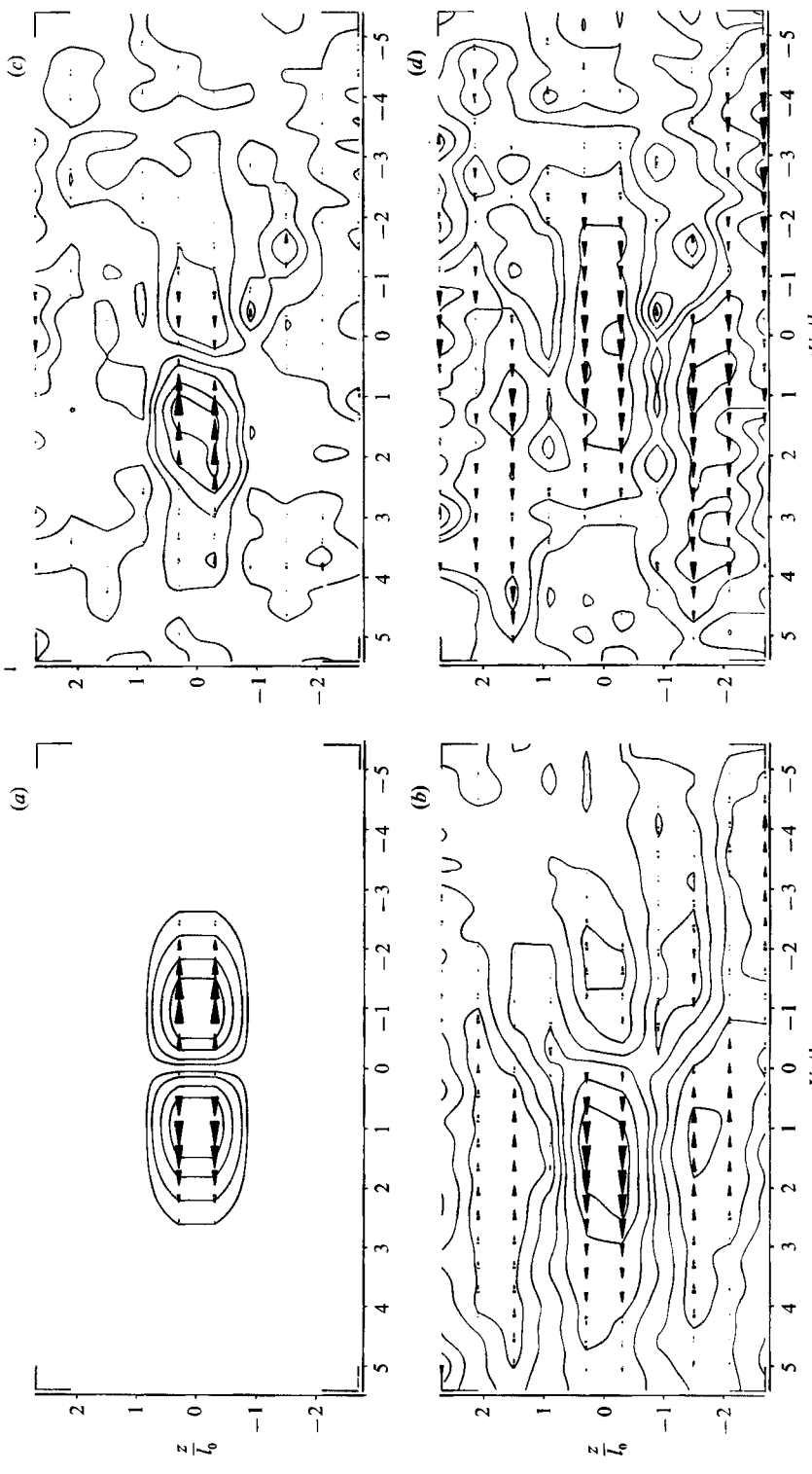

FIGURE 5. Structures linked to fast-to-slow velocity gradients in the horizontal plane: (*a*) template, (*b*) ensemble average, (*c*) $\langle U^2 \rangle$ ensemble average, (*d*) $\langle U^2 \rangle - \langle U \rangle^2$ ensemble average.

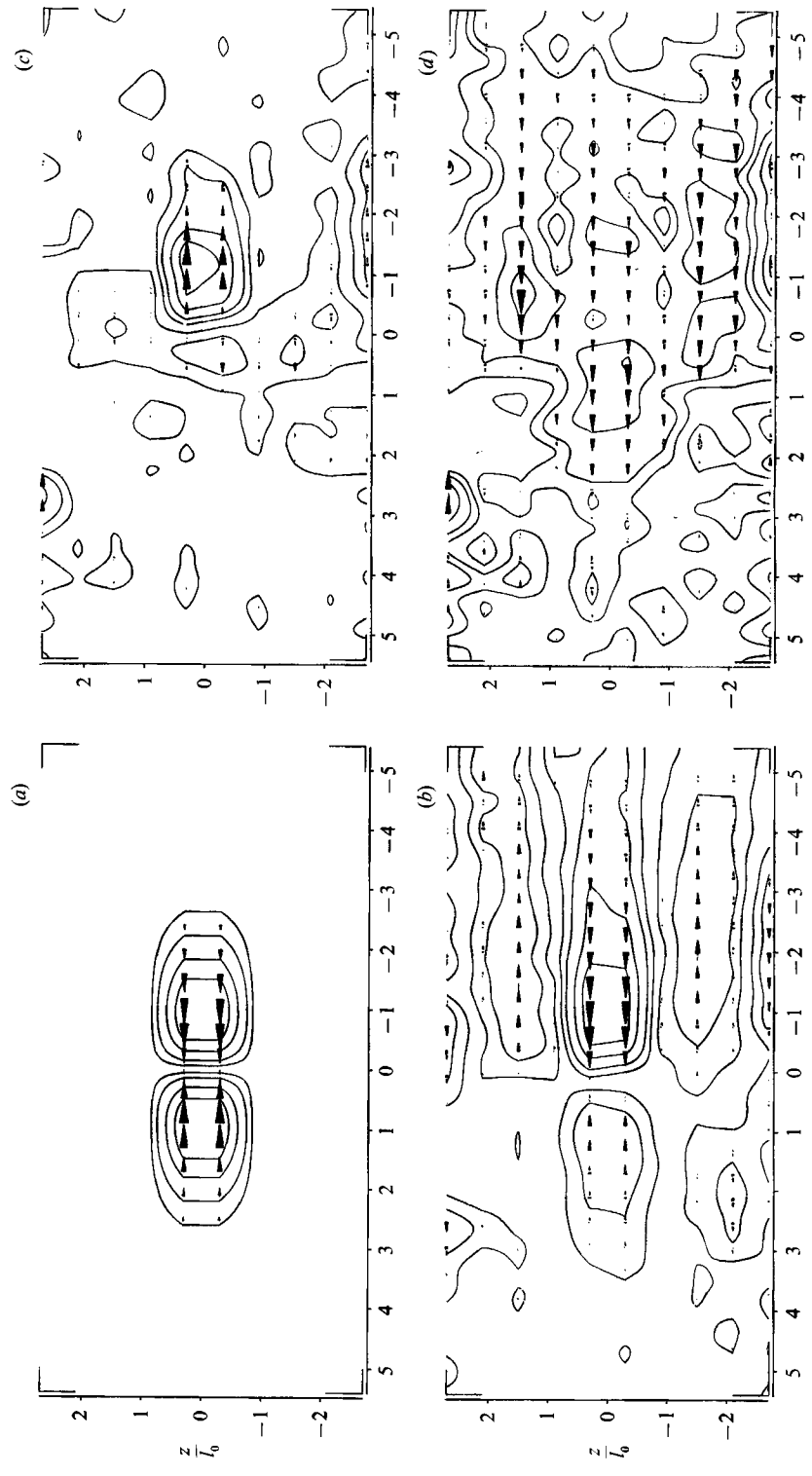

FIGURE 6. Structures linked to slow-to-fast velocity gradients in the horizontal plane: (*a*) template, (*b*) ensemble average, (*c*) $\langle U^2 \rangle$ ensemble average, (*d*) $\langle U^2 \rangle - \langle U \rangle^2$ ensemble average.

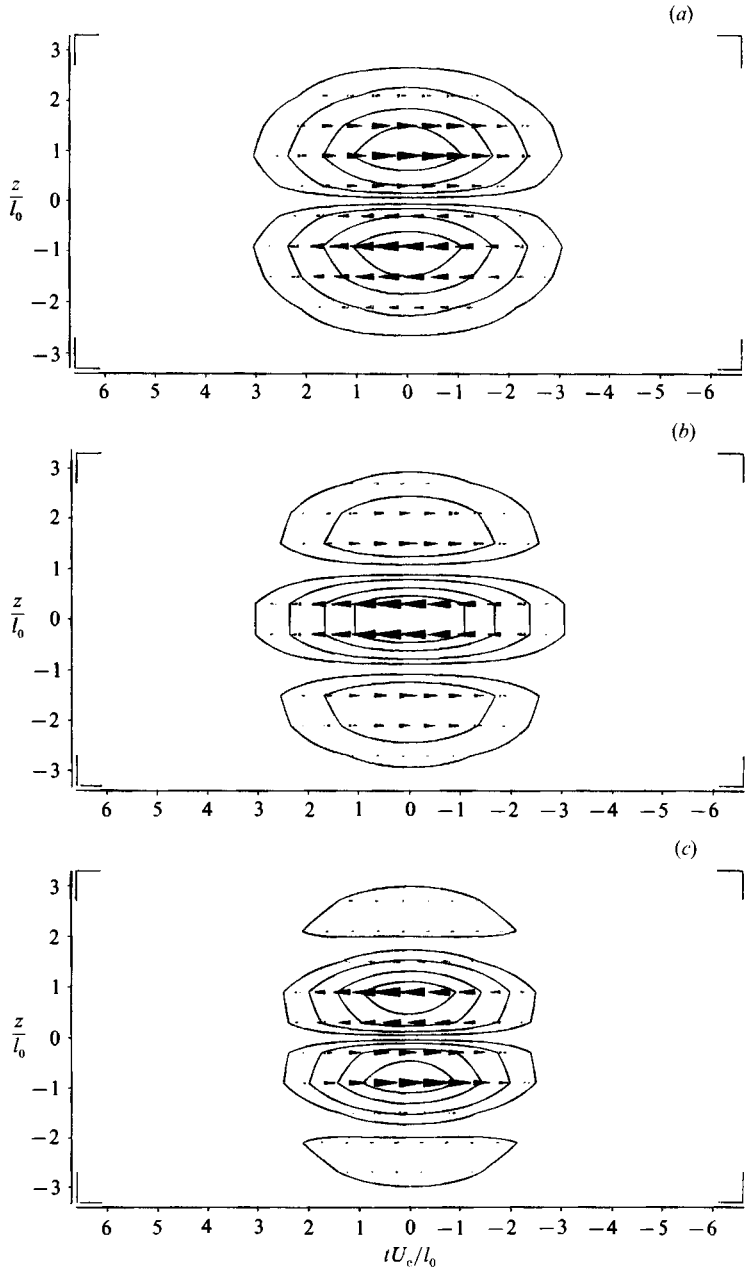

FIGURE 7. Comparison of (*a*) the stream function, (*b*) the u-velocities and (*c*) the vorticity footprints of a double-roller eddy.

analysis. It can be observed in this figure that the core of vorticity, composed of two cells with opposed circulation, does not involve as many anemometers as the u-velocity footprints of the double roller seem to suggest in figure 7(*b*).

The temperature data already examined in FG2 have been analysed again to confirm the actual size of the hot spots associated with temperature gradients in the heated wake. Results obtained are presented in figure 8. Figures 8(*a*) and 8(*c*) are the

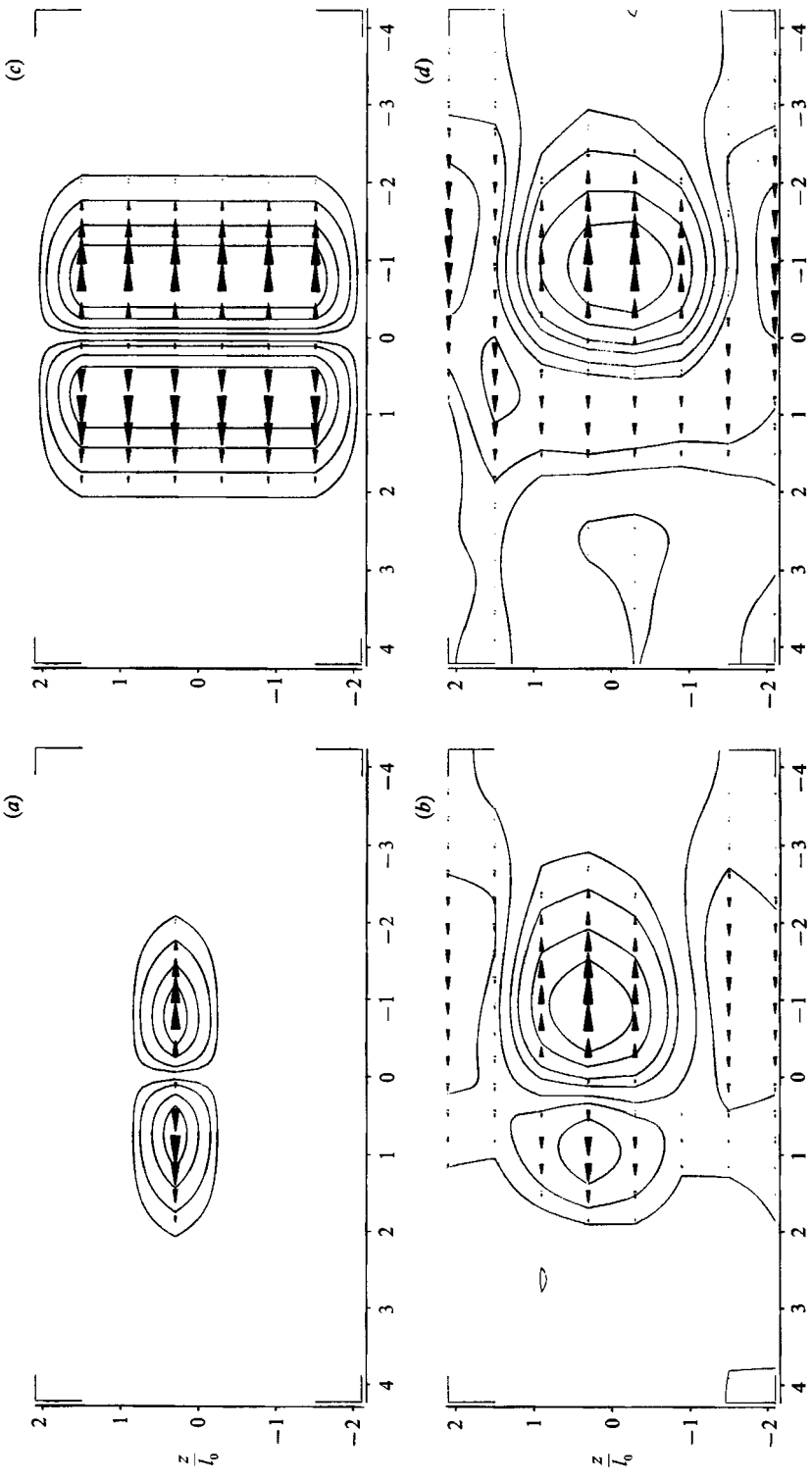

FIGURE 8. Hot-to-cold temperature gradients in the horizontal plane of the thermally contaminated wake: (*a*) template involving a single thermometer, (*b*) ensemble average obtained from (*a*), (*c*) template involving six thermometers, (*d*) ensemble average obtained from (*c*).

two initial templates; one of them, figure 8(*a*), corresponds to a temperature gradient sensed by a single anemometer, while the other, figure 8(*c*), is a temperature gradient involving simultaneously six contiguous thermometers. The final patterns, figures 8(*b*) and 8(*d*), both show that typical temperature fronts appear simultaneously in three or four anemometers, with a width of 1.2–1.8 l_0 units, approximately.

What is important to note is that what we call the core of vorticity in figure 7(*c*) matches very well the size of the hot spots in either figures 8(*b*) or 8(*d*). This explains the apparent mismatch in size between temperature and velocity patterns. Temperature (hotter fluid) can be thought to be confined in the core of vorticity, irrespectively of its sign, yielding typical footprints over approximately four anemometers (figures 8b and 8*d*). The footprints of the same eddy when observed as velocity fronts (slow-to-fast velocity gradients in figure 6*b*) involve only the two anemometers sensing the central part of the eddy, which is consistent with the simulated footprints of velocity and vorticity plotted in figure 7. Therefore, the streamwise velocity gradients and the temperature fronts can be associated with the passage over the set of anemometers of the same kind of organized structures: the double-roller eddies with a backflow in their centres.

4.3. *The double-roller eddies in the vertical plane of the wake*

During the analysis of the velocity signals obtained in the vertical plane of several wakes (FG1), the data were scrutinized for organized motions with vorticity aligned with the cylinder axis, which were termed Kármán-like or ω_z-vortices. In the wake of a single cylinder these were clearly detected up to $x/D = 60$. At $x/D = 140$ for the same wake and in many of the other wakes examined, the ω_z-vortices were observed to be strongly dominated by shear alignment. In addition, the temperature signals in the vertical plane (FG2) showed clearly that the typical organization of the thermal field was temperature fronts aligned with the shear and covering the whole width of the wake. This set of results, plus those obtained when looking for velocity gradients in the horizontal plane, indicated the need for re-examining the typical organization of the velocity field in the vertical plane. In order to give more importance to the shape of the double roller rather than to their actual velocity patterns, the data for each anemometer were normalized using the individual r.m.s. values instead of a pooled estimate, as mentioned before. In addition, a velocity pattern that could be easily related to the temperature patterns of FG2 and to the velocity patterns in the horizontal plane (figures 3, 5 and 6) was selected.

The templates used are presented in figures 9(*a*) and 10(*a*). They are the vertical counterparts of figures 5(*a*) and 6(*a*), respectively, a velocity gradient showing fast-to-slow and slow-to-fast transitions located at the maximum shear stress position. The results obtained are presented in figures 9(*b*, *c*, *d*) and 10(*b*, *c*, *d*), showing the intermediate patterns produced at each iteration. The most relevant feature when the initial and final steps are compared, is that the flow organization linked to the velocity gradients that occur at the maximum shear stress position are velocity fronts spanning the whole width of the wake which are extremely similar to the temperature fronts detected in the thermal field of the wake (FG2). In fact, they are rather more than just similar. Indeed it can be said that the ensemble averages of figures 9(*d*) and 10(*d*) should be the velocity patterns associated to the temperature fronts observed in the thermal field, because velocity and temperature fluctuations are always correlated with the same sign across the wake. The correlation is negative because the negative velocities correspond to the old, turbulent flow that in a thermally contaminated wake is hot, while the positive velocity fluctuations are

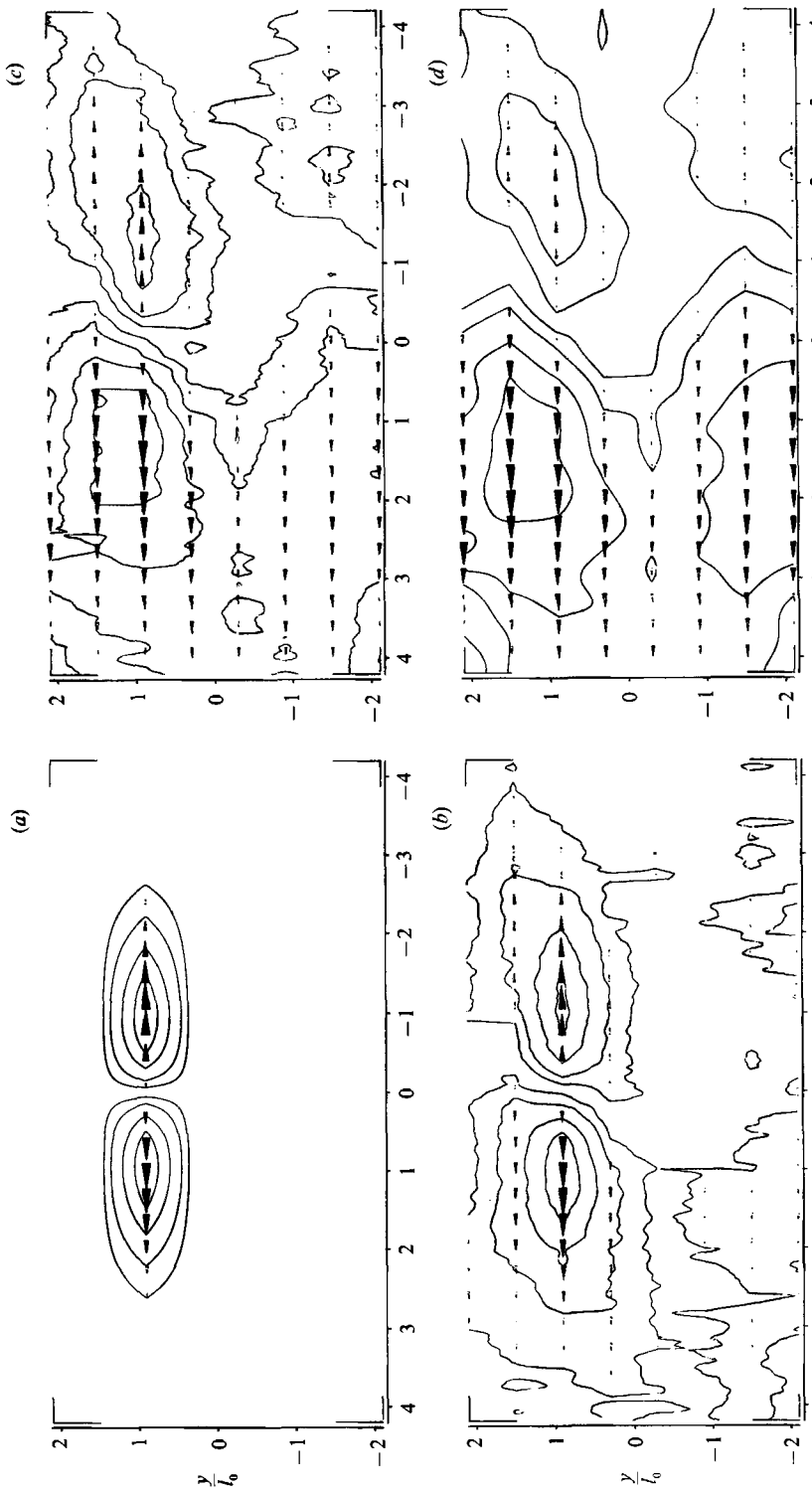

FIGURE 9. Structures linked to fast-to-slow velocity gradients in a vertical plane: (*a*) template, (*b*) ensemble average after one iteration, (*c*) ensemble average after two iterations, (*d*) ensemble average after three iterations.

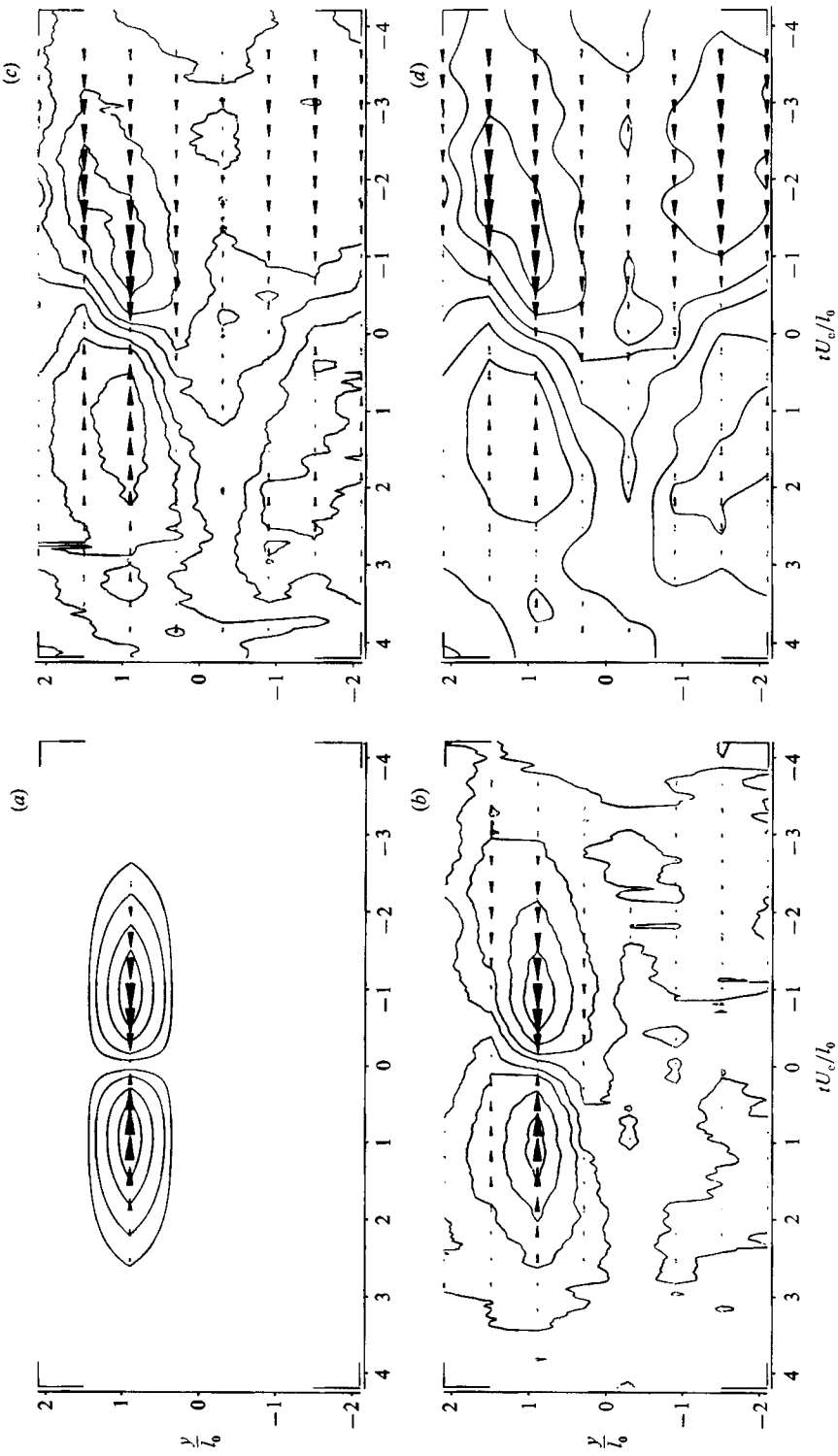

FIGURE 10. Structures linked to slow-to-fast velocity gradients in a vertical plane: (*a*) template, (*b*) ensemble average after one iteration, (*c*) ensemble average after two iterations, (*d*) ensemble average after three iterations.

produced by the newly entrained potential flow, which is cold (or at least 'colder' than the mean flow) and carries momentum into the wake contributing to the transfer of energy from the free-stream flow to the turbulent core of the wake.

The results obtained in the horizontal plane, figures 5 and 6, linked the double-roller eddies to the streamwise velocity gradients. Hence figures 9(*d*) and 10(*d*) also have to be interpreted as the side view of the double-roller eddies. The final pattern seems to suggest the hypothesis that the double rollers tend to appear simultaneously in both sides of the wake; a detailed analysis of the intermediate iterations gave support to the point of view of Mumford (1983), who suggested that some of the double rollers could appear symmetrically in both sides of the wake. Nonetheless, some of them seemed to be confined to only one half of the wake. It is evident from figures 9(*b*) and 10(*b*) that after only the first iteration weak evidence is obtained of organization crossing the wake. In the following iterations, figures 9(*c*, *d*) and 10(*c*, *d*), both sides of the wake become more and more similar, partially because the double rollers that cross the wake achieve a better alignment as soon as negative velocities appear in the bottom half of the pattern, partially because an unpaired double roller located in the bottom of the wake begins to contribute to the ensemble average only when negative velocities appear in the bottom half of the averaging data window.

It is worth noting that figures 9(*d*) and 10(*d*) display some differences which seem to be associated with the singular features of the trailing and leading edges of the double-roller eddies, like those observed in figures 5(*b*) and 6(*b*). However, now these differences appear clearly linked to the outermost anemometers, that is, those placed in the edges of the wake. This problem is again related to the tops of the double rollers, as pointed earlier. Finally, we would like to point out that in both figures 9(*a*) and 10(*a*), from an initial pattern containing positive and negative velocities, the pattern recognition procedure yields ensemble averages dominated by the negative velocity organization, a result that gives further support to the conclusion that a preponderance of double-roller eddies with backflow in the centre exists in the wake.

Although the velocity patterns observed in the vertical plane have been interpreted as a side view of the double-roller eddies previously detected in the horizontal plane, the frequency at which the double rollers are detected in the horizontal and vertical planes does not show the same distribution. The histograms corresponding to the ensemble averages of the double rollers in the horizontal plane, figure 3(*b*), and of the double rollers associated with slow-to-fast velocity gradients, figure 6(*b*), as well as the side view of the double-roller eddies, figure 10(*d*), are presented in figures 11(*a*), 11(*b*) and 11(*c*) respectively. All histograms in these figures and in figure 13 have been obtained using the total length of sampled data. It can be observed that the double rollers are detected in the horizontal plane, approximately with the same frequency irrespective of whether the central velocity lobe is associated with streamwise velocity gradients or not. However, comparison of figures 11(*c*) and 11(*b*) shows a significant shift of activity towards lower frequencies in the histogram of the vertical-plane data.

The explanation for this shift in activity of the detection frequency may be that the double-roller eddies tend to occur in groups, filling up the turbulent bulges, so that they contain from one to four double-roller eddies. In the horizontal plane at the maximum shear stress position where these eddies seem to play a very strong role, the detection procedure used should be able to detect all of them one by one and thus yield a detection frequency that would show activity centred at two different zones: one representative of the distance between consecutive double rollers at higher

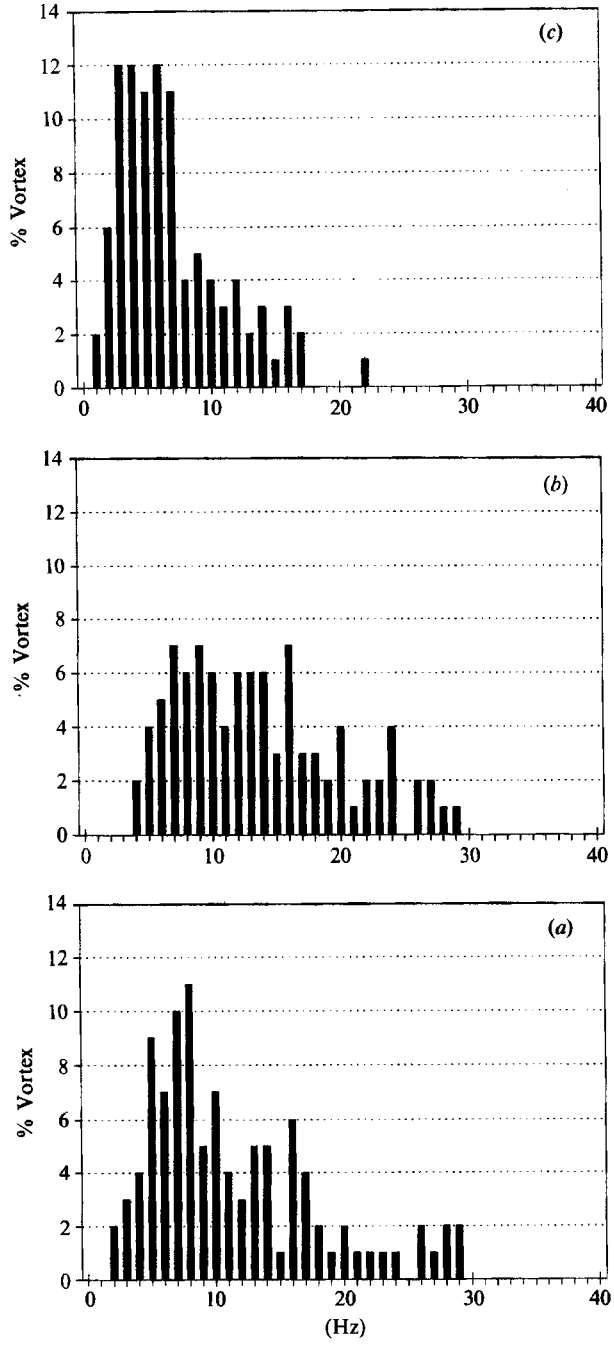

FIGURE 11. Histogram of the detection frequency of double-roller eddies: (*a*) horizontal plane (ensemble average shown in figure 3*b*), (*b*) horizontal plane (ensemble average shown in figure 6*b*), (*c*) vertical plane (ensemble average shown in figure 10*d*).

frequencies, the other representative of the separation between consecutive turbulent bulges at lower frequencies. However, in the vertical plane, as a consequence of using information that involves simultaneously the whole width of the wake, the procedure would not be expected to detect the individual double rollers. Only the first or the last in each package, i.e. only those directly involved in featuring the boundaries of the turbulent bulges, should be detected. If this were the case, the detection frequency in the vertical plane should be centred mainly at low frequencies, as is observed.

4.4. *The tops of the double-roller eddies*

With all this information to hand, one is tempted to draw a sketch of what could be the three-dimensional large-scale organization of the flow in the form of double-roller eddies and their relation with the turbulent/non-turbulent interface and the process of entrainment by engulfing. However, there is a piece of information missing in this puzzle and this concerns the top of the rollers. Are the two eddies of a double roller connected at their top forming some kind of big horseshoe as hypothesized by Savill (1979)? If so what role do these tops play in the entraining process and are they the LASMOS (Large Anisotropic Swirling MOtionS) as he suggested?

Only a partial answer to these questions can be given on the basis of the results obtained so far during the analysis of the data in the vertical plane. All the ensemble averages in this plane showed the dominance and importance of the negative velocity fluctuations, which we have interpreted as the side view of double rollers. If these were connected on top forming a horseshoe, the velocity footprints of the tops of the rollers should be located only in the anemometers more towards the ends of the rake and, to be consistent with the sense of rotation that corresponds to backflow in the centre, the typical velocity patterns should imply positive velocity fluctuations on the top (or bottom) of the wake accompanied by negative velocities in the more central anemometers. This is the template shown in figure 12(*a*). The intermediate results and the final pattern obtained are presented in figure 12(*b*, *c*, *d*) after running the pattern recognition programs for three iterations. It can be observed how the first iteration produces an ensemble average consistent with our hypothesis. However, in the following iterations the negative velocities are of more and more importance, yielding an ensemble that becomes similar to that of figure 9(*d*) or 10(*d*). This effect can be clearly attributed to a loss of selectivity of the procedure owing to the appearance of the negative velocities that characterize a region of the central part of the rollers at least $0.60\,l_0$ units wide (see figure 3*b*).

If the detection frequency just after the first iteration, figure 13(*a*), is examined and compared with that observed in the third iteration, figure 13(*b*), it is possible to answer some questions regarding the validity of our hypothesis about the tops of the double rollers. It is clear that the detection frequency corresponding to the ensemble average of figure 12(*d*), that is the histogram of figure 13(*b*), is consistent with the detection frequency previously observed in the vertical plane, figure 11(*c*). But the histogram after the first iteration, figure 13(*a*), is similar to the more selective detection in the horizontal plane, figure 11(*a*, *b*). Therefore, despite the fact that we have to stop the iterative procedure to obtain strong evidence about the tops of the double rollers, the histogram tells us that the search in the first iteration is as effective and exhaustive as it was in the horizontal plane when looking for slow-to-fast velocity gradients. The number of data windows averaged to obtain figure 12(*b*) is approximately two times the number of patterns averaged in figure 12(*d*). When

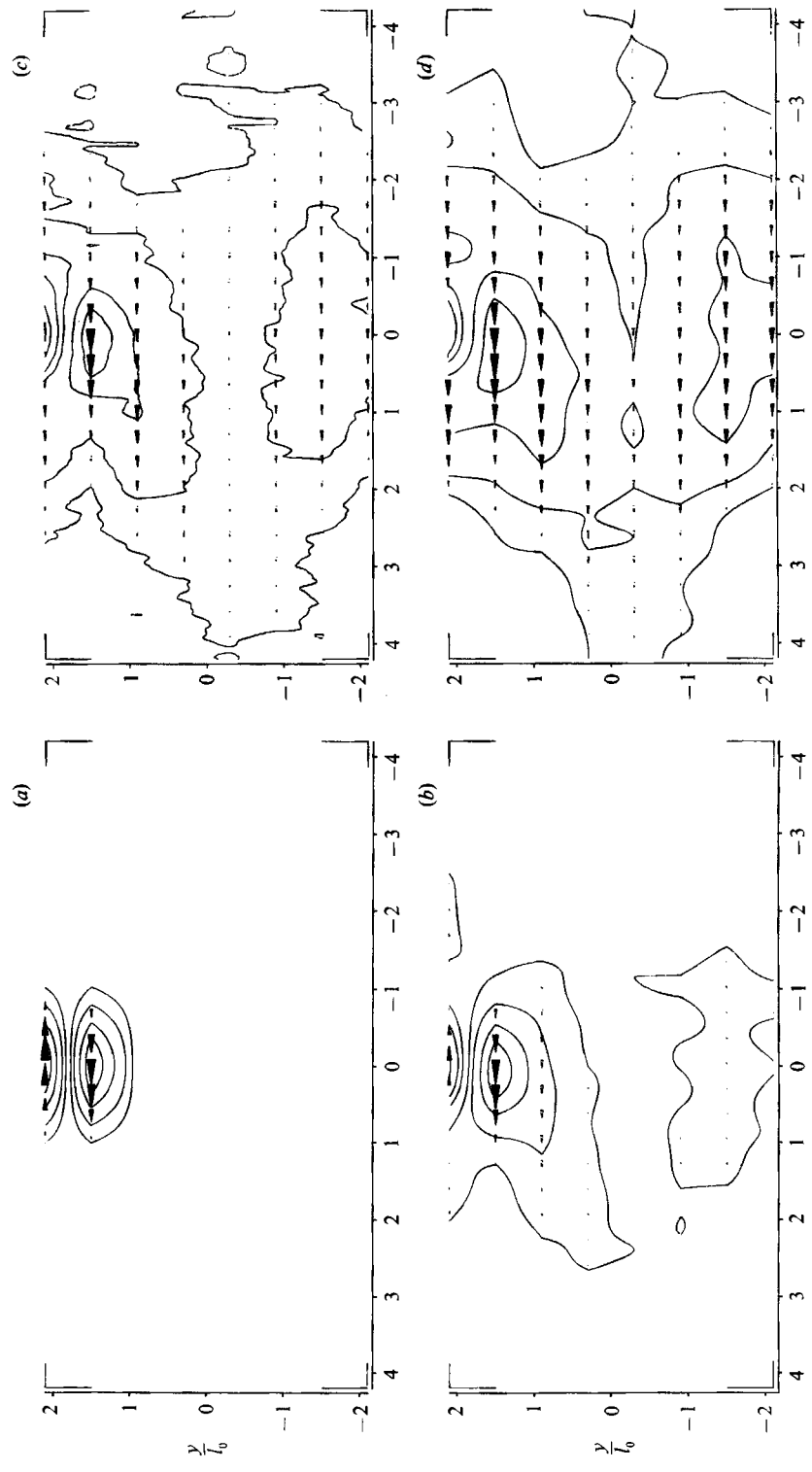

FIGURE 12. Velocity patterns of the top of the double-roller eddies: (*a*) template, (*b*) ensemble average after one iteration, (*c*) ensemble average after two iterations, (*d*) ensemble average after three iterations.

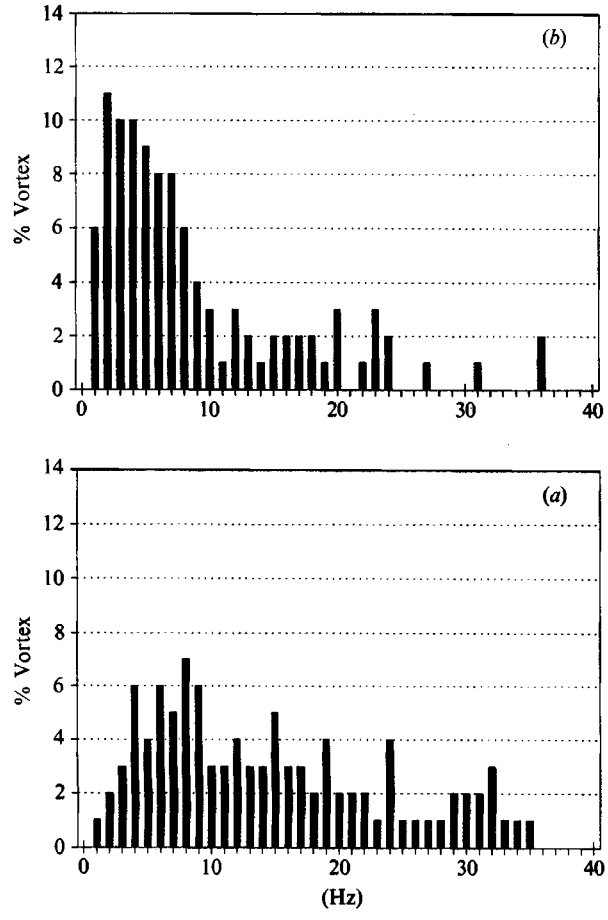

FIGURE 13. Histogram of the detection frequency of the velocity patterns associated with the top of the double-roller eddies: (*a*) after one iteration (ensemble average shown in figure 12*b*), (*b*) after three iterations (ensemble average shown in figure 12*d*).

this is taken into account the histograms of figure 13(*a*, *b*) become even more dissimilar because the shift towards lower frequencies of figure 13(*b*) means that in fact only a small fraction of the high-frequency patterns are averaged.

All the information obtained so far can be put together to form the picture presented in figure 14. Figure 14(*a*) shows some details of the double-roller eddies. These are formed by two counter-rotating vortices that sometimes appear only in one side of the wake, but which occasionally also appear to cross the wake. Moreover, the two vortices in a double-roller eddy are not independent, but are connected at the top forming a horseshoe structure. Such a hypothesis is based on the results presented in figure 12, but mainly on the shear alignment displayed by the organized motions observed in the heated wake. Also the role played by the double-roller eddies in the process of entrainment by engulfment (FG2) seem to support this three-dimensional picture. Results reported elsewhere (Ferré, Giralt & Antonia 1989) indicate that vorticity parallel to the cylinder axis exists linked to the double rollers.

Figure 14(*b*) is an attempt to describe how the double-roller eddies are related to the turbulent/non-turbulent interface in the far wake. The arrangement presented is not the only one possible because the random character of the flow permits many

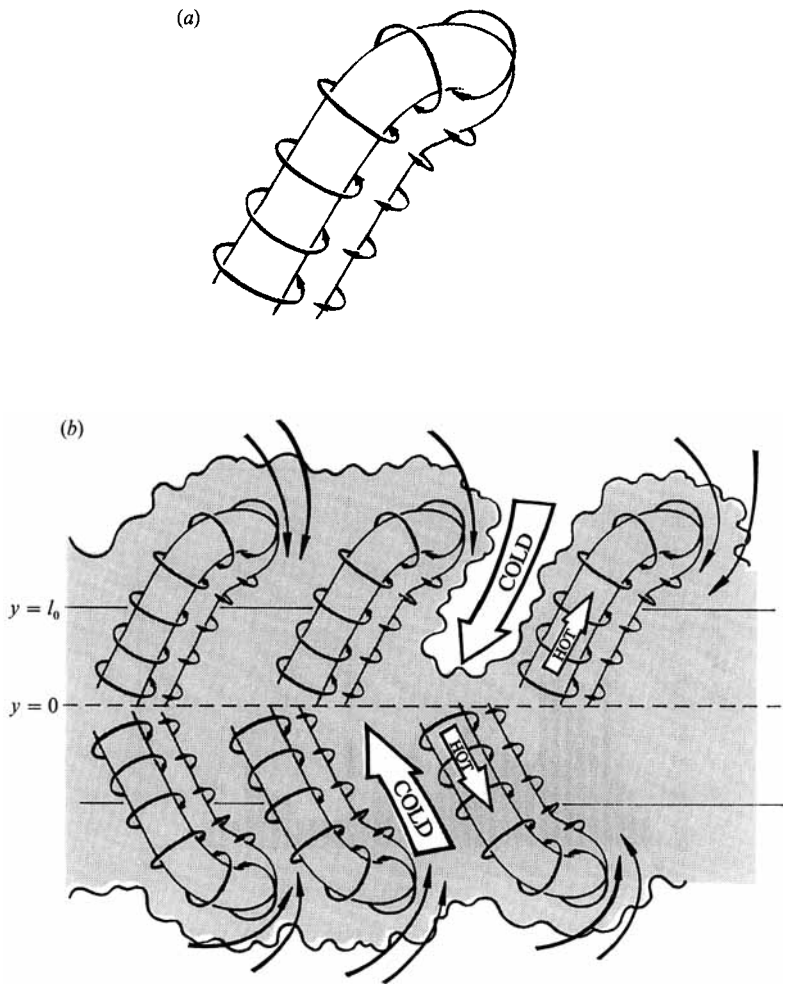

FIGURE 14. Three-dimensional sketch of entraining motions: (*a*) a double-roller eddy, (*b*) instantaneous vertical slice of the far wake.

other assemblies of the basic building blocks, but it is consistent with previous observations that both double rollers and entraining motions tend to occur in groups of three to five. Three double rollers are presented filling a big turbulent bulge in the wake. The fast-to-slow and slow-to-fast patterns in both the horizontal and vertical planes would be the characteristic velocity footprints of the leading and trailing edges of the double roller, respectively. These are also responsible for the appearance of the temperature fronts in the far wake of a heated cylinder (FG2). The strongest temperature fronts are the hot-to-cold transitions of the trailing edge of the rollers, while the cold-to-hot fronts are never so clearly defined or steep because of the entrainment of potential flow induced by the top of the rollers. The leading double roller in the turbulent bulges may be the one primarily responsible for the entrainment by engulfing, while the central and trailing rollers could be more active in a scale intermediate between the molecular diffusion and the engulfing, which might be termed 'nibbling'.

The picture presented is by no measn just a 'side view' of the wake. As a consequence of the strong three-dimensional character of the double rollers this is just one slice of the flow, while in parallel slices one could expect to observe similar organizations, but out of phase. The turbulent bulges as well as the patches of potential flow entrained should have an extent in the spanwise direction of the same order of magnitude as that in the streamwise coordinate. Instead of being arranged just one behind the other, the double-roller eddies seem to be ordered into a staggered arrangement, as suggested by the detection of a very strong 'patched' organization in the thermal field (Ferré 1986).

Grant (1958) postulated the existence not only of the double-roller eddies, but he also identified 'mixing jets' that were transporting fluid from the centre of the wake towards the potential flow. These 'jets' might be identified with the double-roller eddies, or more precisely, with the upper sections of the double rollers as they move away from the centre of the wake. The conditional-sampling measurements of Fabris (1979) shed some light on this question. His conditional mean v-velocities were observed to indicate the continuous movement of hot fluid all across the wake away from the centreplane, and a corresponding movement of cold fluid towards the centre of the wake. This observation leads to a final point related to figure 14 and the double-roller eddies. Despite the fact that most of the flow in the far wake seems to be full of double rollers, these larger eddies cannot be a 'static' organization of the flow. They have to have a life cycle, with a generating mechanism originating, probably, in a zone near the centre of the wake, and a growth and decay cycle. They would then be equilibrium eddies, not only in the energetic sense, losing and gaining energy simultaneously, but in a continuous dynamic equilibrium between growth and decay.

4.5. *Contribution of the double-roller eddies to the r.m.s. values*

There are several ways to quantify the importance of the double-roller eddies in the far wake. Obviously, one of them is to evaluate the fraction of flow represented by the ensemble averages. This can be done by computing the ratio of data points that make an ensemble average to the total number of points analysed. The values obtained for all the results presented are in table 1. Usually these values are about 40%–50%, a value that is consistent with the life-cycle point of view expressed above.

A second way to evaluate the role of the double rollers in the wake is to compute modified statistics of the velocities after accounting for the double rollers detected, as discussed earlier. The results obtained are presented in table 2 for the case of the double-roller eddies detected in figure 6(*b*). Obviously, if the double rollers were removed from the wake, the small-scale motions would change, as we intend to show in the second part of the paper. However, at least a rough estimate can be obtained by subtracting their mean effect. It can be observed that the double rollers can account for about 40% of the energy contained in the u-velocity fluctuations, a level which shows the extremely important role played by the double rollers in the far wake.

The anemometers that achieve a highest reduction are those in the centre of the rake because most of the double rollers they are sensing are classified, while the anemometers in the edges of the rake would be more influenced by the double rollers that are out of the data because they have been swept only partially over the anemometers. The contribution of the double-roller eddies to the r.m.s. values of the

		Significance (%)			
Figure	% Flow	Figure (*a*)	Figure (*b*)	Figure (*c*)	Figure (*d*)
3	46	—	1.7	18.2	42.9
				(0.02)	(4.8)
4	40	—	6.8	26.7	35.7
			(0.0)	(0.6)	(2.1)
5	45	—	3.0	27.2	48.0
				(0.6)	(8.1)
6	45	—	1.9	18.8	50.8
				(0.1)	(9.8)
8	60	—	—	0.0	0.0
9	43	—	—	—	10.0
					(0.0)
10	45	—	—	—	10.0
					(0.0)
12	40	—	0.2	—	20.0
					(3.6)
15	46	1.7	46.0	—	—
			(6.0)		
16	45	1.9	50.0	—	—
			(9.0)		
17	45	10.0	10.0	10.0	43.0
		(0.1)	(0.0)	(0.0)	(5.0)
18	43	10.0	1.7	0.4	35.0
		(0.0)			(2.0)

TABLE 1. Significance levels of the $\pm 10\%$ contour in the ensemble averages and fraction of flow classified

Note: significance level of the $\pm 25\%$ contour is added below in parentheses when the value attained by the $\pm 10\%$ contour is more than 5%

temperature signals has been evaluated when running the pattern recognition analysis to produce figure 8. These values are also presented in table 2, where it can be observed that the reduction in turbulent activity in the thermal wake is also more than 30%.

4.6. *Comparison with other experiments*

A slightly different picture of the far wake has emerged recently from the work of Antonia and coworkers using a conditional-sampling technique. Our discussion will be centred mainly on Browne *et al.* (1986), though a more complete set of results is presented in Antonia *et al.* (1987). Before explaining how their results fit in the picture we have been building up, we should discuss the details of the conditional-sampling procedure they used in view of the findings we have presented in the previous sections. The experiment described in their paper was carried out in a thermally contaminated wake, the detection signal was obtained by a set of thermometers placed in a spanwise arrangement, while the conditional averages were obtained using a $\times$-wire that measured u- and v-velocities in a vertical plane. The averages of u- and v-velocities were conditioned by the detection of spanwise temperature fronts simultaneously sensed by the set of four anemometers.

We know from the results presented here and those previously presented in FG2, that the temperature fronts that occur in the z-coordinate of the flow are associated

Sensor	Velocity field (figure 6) $\overline{u_R^2}/\overline{u^2}$	Thermal field (figure 8) $\overline{\theta_R^2}/\overline{\theta^2}$
1	0.66	0.67
2	0.65	0.67
3	0.62	0.66
4	0.61	0.66
5	0.62	0.66
6	0.62	0.67
7	0.66	—
8	0.65	—

TABLE 2. Contribution of the double-roller eddies to the r.m.s. values in the far wake ($x/D = 140$) at the maximum shear stress position

with the central part of the double roller, that is, the sharp hot-to-cold temperature fronts of figure 8(*d*) are the slow-to-fast velocity gradients of figure 6(*b*), which in turn are undoubtedly identified with the centre of the double-roller organization. By rejecting any temperature front not occurring simultaneously in the four anemometers, Browne *et al.* (1986) were taking exactly conditional samples in a vertical plane centred in the double-roller eddies, hence their u- and v-velocity patterns are a high-quality version of the u-velocity patterns observed in the first iteration of figure 12(*b*).

There are some features in figure 4 of Browne *et al.* (1986) that seem to be incompatible with the picture we have been offering of the far wake. However, a closer look at the details of the conditional-sampling approach they were using reveal that this is not the case. First, they present a picture of groups of three eddies because the detection criterion is to select a temperature front only when this is preceded and followed by other temperature fronts. As they explain, if this is not the case the ensemble average results will be smeared out in the edges of the averaging window. This is exactly the same problem as has been previously discussed concerning the differences between the patterns and histograms in the vertical and horizontal planes and led us to the similar hypothesis that groups of double rollers form the big turbulent bulges in the wake.

A second aspect that is more difficult to reconcile with our experimental evidence is the antisymmetric arrangement of temperature fronts in the wake. Once again figure 4 of Browne *et al.* (1986) presents such an arrangement because this is a feature selected during the stage of accepting, or not, a set of three consecutive temperature fronts as triggering signal. But a simple calculation based on the number of points presented in their data windows and the total length of the records they used shows that this configuration is representative of only approximately 15% of the flow.

During the analysis of the thermal field of the far wake, the hypothesis of an antisymmetric arrangement was tested (see figure 4 in FG2) but a final pattern was obtained that was very similar to the symmetric arrangement. In addition, the velocity field in the vertical plane (figure 10 in this paper) shows a clear tendency towards symmetric arrangements. Perhaps neither of these two extreme descriptions represents the true picture. Indeed our point of view is that there are some double rollers that appear crossing the wake centreline, giving rise to the symmetric arrangement, while the double rollers appearing only in one side of the wake are

independently distributed. However, as the existence of a non-connected double roller on one side of the wake does not preclude the existence of a second double roller in the other side, this random distribution plus the order imposed by the double roller crossing the wake may give rise to a mixture of connected and randomly distributed non-connected double rollers that could resemble an antisymmetric arrangement. Apart from these discrepancies, it is extremely important to recognize that the ensemble averages of Browne *et al.* (1986) correspond to a strongly three-dimensional flow organization, since it is the criterion adopted to make use of the triggering signal based on temperature fronts simultaneously occurring in the spanwise-aligned anemometers.

The velocity patterns of Browne *et al.* (1986) displayed in their figure 4 have been obtained assuming a constant convection velocity across the wake. This approach is different to ours in the sense of centring the analysis only in the deviations from the conventional means. As pointed out when discussing the normalization of the velocity signals, assuming a constant convection velocity across the wake will result always in obtaining excess velocities in the edges of the wake and negative ones in the centre. This is the reason why the velocity patterns displayed by Browne *et al.* (1986) are much bigger than one would expect if they were the tops of the rollers. However, if corrections were made to avoid this effect, it would probably be observed that the entraining motions appearing above what they call the diverging separatrices, are in fact the tops of the double rollers.

Another aspect that emerges clearly from the comparison of both experiments is that vortex stretching occurs in the cores of vorticity of the double rollers, along the lines of their diverging separatrices. Otherwise, we suspect that what Browne *et al.* call the converging separatrices would be very sensitive to the selection of the convection velocity. In general it seems that the need for describing the turbulent flow in terms of saddle points and converging and diverging lines arises mainly from the difficulties of drawing a true three-dimensional picture when only slices of the flow in one plane are considered, rather than the whole flow.

5. The fine-scale activity in the far wake

The ensemble averages of the normalized second time derivatives associated with the velocity patterns of the double-roller eddies in the horizontal plane are presented in figures 15 and 16. These correspond to the analysis of figures 3 and 6, respectively. Figures 15(*a*) and 16(*a*) are identical to figures 3(*b*) and 6(*b*), which are repeated to help clarify our analysis. The first thing we should note is the scatter of the isolevel contours of the second derivatives which is consistent with the low significance of the $\pm 10\%$ contour (see table 1). We have to move to the $\pm 25\%$ contour to attain significances of 6% and 9% in figures 15(*b*) and 16(*b*), respectively. However, a number of interesting findings emerge from the plots of figures 15(*b*) and 16(*b*) which could shed some light on the large-scale/fine-scale interactions in the far wake.

First, a higher fine-scale activity is observed linked to the central negative velocity lobes in both ensemble averages. But the more external positive velocity fluctuations induced by the double-roller eddies, which are far away from the vorticity cores, present a clear deficit in the fine-scale activity, attaining values as low as those obtained by the positive velocity fluctuations of the streamwise velocity gradients (see figure 16). These in turn could be identified as true potential or 'just engulfed' potential flow. This means that at the edges of the rollers, where the flow associated with the large-scale motions is in the same direction as the main stream, the flow is

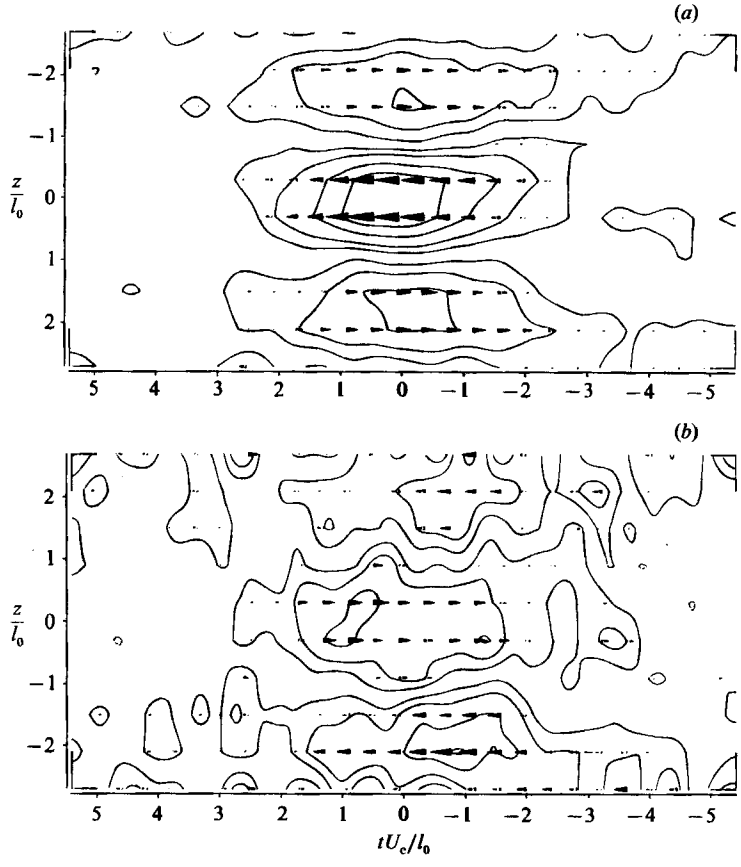

FIGURE 15. Fine-scale activity associated with the double-roller eddies in the horizontal plane: (*a*) ensemble-averaged velocities (figure 3*b*), (*b*) ensemble-averaged envelope of the time second derivatives.

calmer or 'more laminar', while the main turbulent activity seems to be produced by the zones of backflow associated with the organized motions.

It is hard to justify the conclusion that the turbulent activity concentrates in the negative velocity fluctuations unless these were in fact generating local shear layers against the mean flow. If this were the case, then very thin shear layers or vortex sheets would be formed between the two counter-rotating vortices of a double roller, which occasionally could be shed into the main body of the turbulent flow. To be consistent with our findings these vortex sheets must be thinner than $0.6\,l_0$ units, because the hot lobes associated with the streamwise velocity and hence the double-roller eddies, always appear very compact. However, if the vortex sheets were an order-of-magnitude thinner than the rollers, implying scales of the order of tenths of l_0, then they would appear to the temperature signals as cold gusts sensed by individual anemometers embedded in the hot spot that precedes the sharp hot-to-cold back of the double roller. In that case their effect would be to produce a lowering of the value of the ensemble-averaged temperatures but not a deep valley of the type observed splitting the hot spots of figure 8(*c*, *d*).

Despite the scatter of the plots and the fact that there are in the ensemble averages of the double roller two anemometers that are actually sensing zero velocities, it can be observed in figures 15(*b*) and 16(*b*) that there is a tendency for the lobe of higher

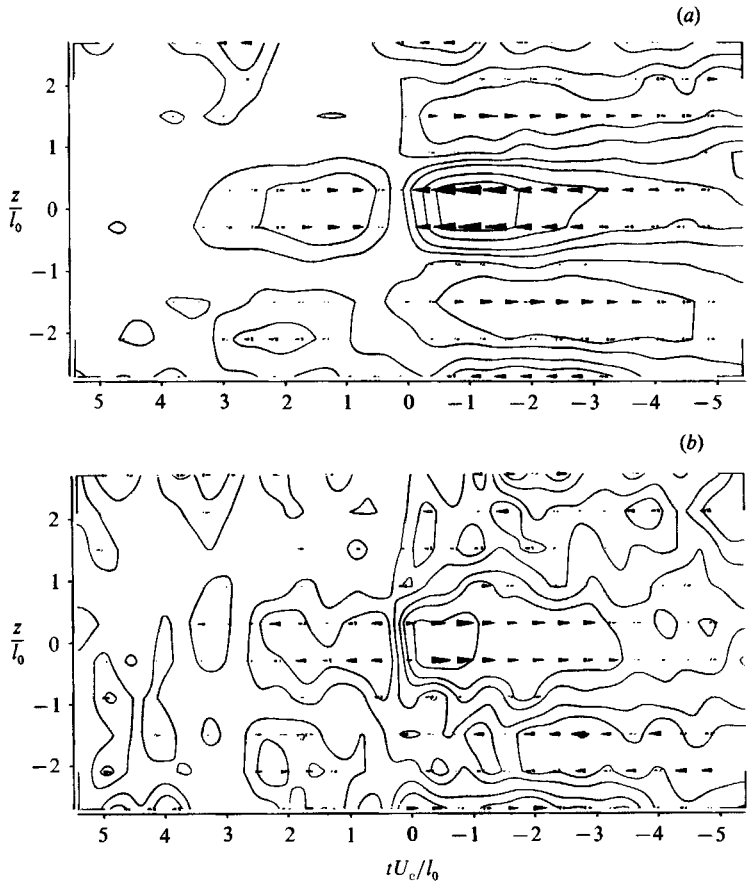

FIGURE 16. Fine-scale activity associated with the double-roller eddies in the horizontal plane: (*a*) ensemble-averaged velocities (figure 6*b*), (*b*) ensemble-averaged envelope of the time second derivatives.

second derivatives in the centre of the patterns to expand to involve more than just the two central anemometers. This observation fits very well with the comparison we did in the last section between the vorticity and temperature patterns in the far wake, suggesting perhaps that the fine-scale activity should be directly linked to the vorticity cores of the double rollers. Moreover, the maximum contribution to the r.m.s. activity (figures 3*c* and 6*d*) comes also from the central anemometers. Obviously in this case only two anemometers appear to be involved because the two extra anemometers bounding the central lobe traverse the rollers near the centres of the two counter-rotating lobes, sensing zero u-velocities in a position where the v- and w-velocities (depending on the actual plane of circulation of the double-roller eddies) should be maximum.

Before proceeding further in our discussion on why and where the fine-scale activity is located in relation to the double-roller eddies, it would be helpful to examine the extra information on the side view of the double rollers that was not presented in figure 9 or 10, where only the velocity field was shown. Figures 17 (*a*) and 18 (*a*) display the final iterations of the pattern recognition analysis (these are figures 9*d* and 10*d* repeated only for the sake of comparison). Figures 17 (*b*) and 18 (*b*) show the $\langle U^2 \rangle$ ensembles averages, figures 17 (*c*) and 18 (*c*) the corresponding $\langle U^2 \rangle - \langle U \rangle^2$

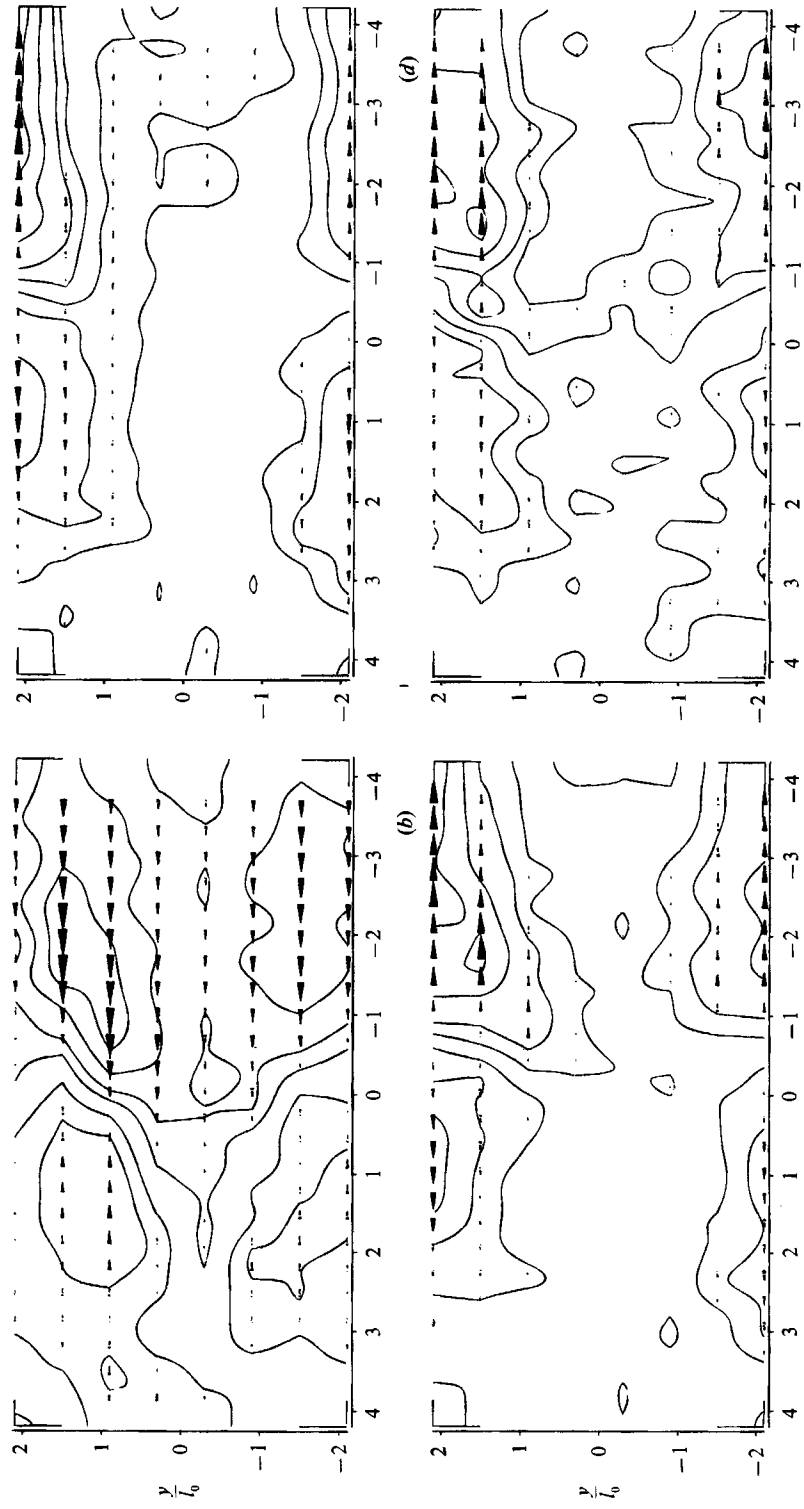

FIGURE 17. Ensemble averages of squared velocities and fine-scale activity detector in the vertical plane: (*a*) ensemble-averaged velocities (figure 10*d*), (*b*) $\langle U^2 \rangle$ ensemble average, (*c*) $\langle U^2 \rangle - \langle U \rangle^2$ ensemble average, (*d*) fine-scale activity detector.

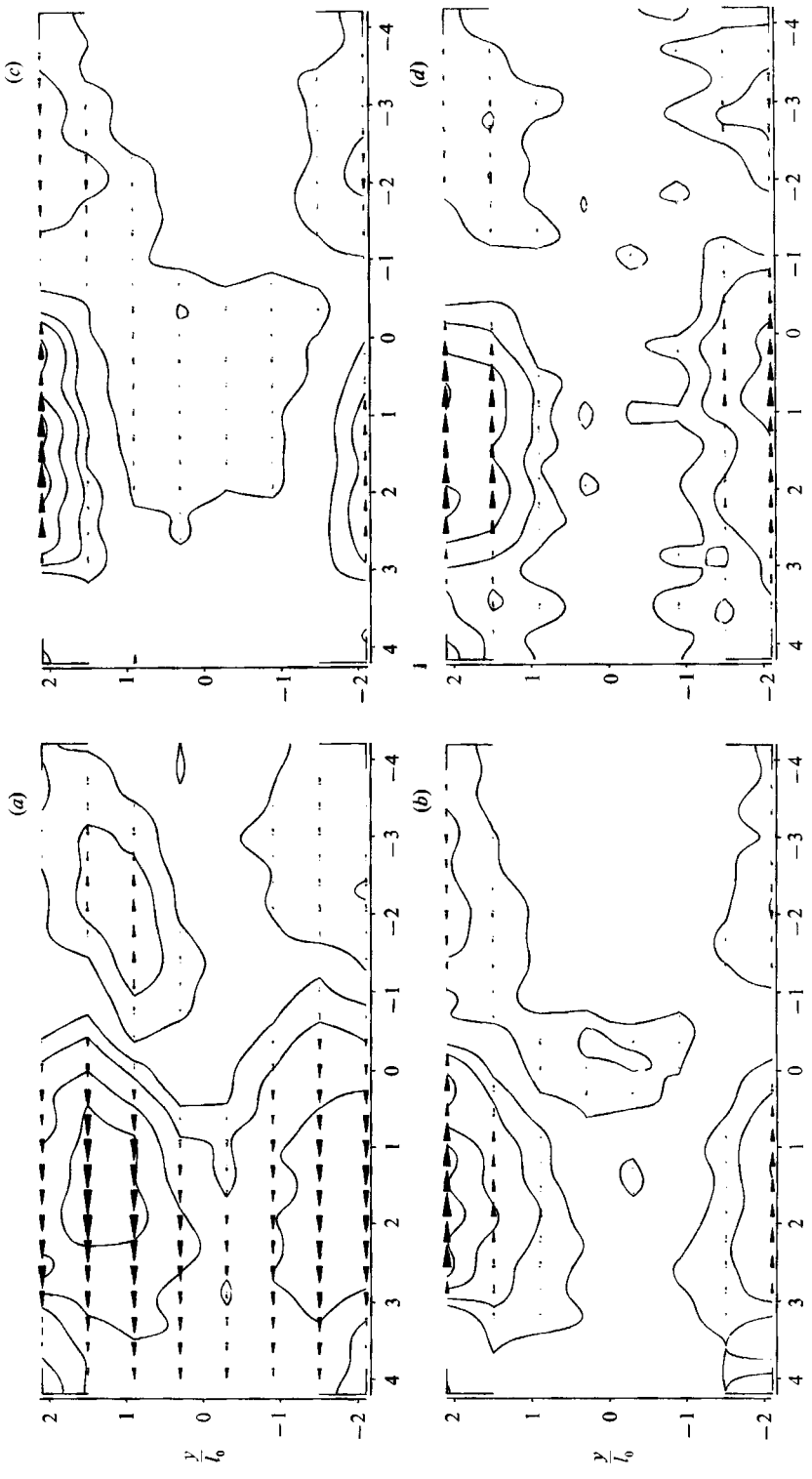

FIGURE 18. Ensemble averages of squared velocities and fine-scale activity detector in the vertical plane: (*a*) ensemble-averaged velocities (figure 9*d*), (*b*) $\langle U^2 \rangle$ ensemble average, (*c*) $\langle U^2 \rangle - \langle U \rangle^2$ ensemble average, (*d*) fine-scale activity detector.

patterns and, finally, figures 17(*d*) and 18(*d*) show the ensemble averages of the envelope of the second derivatives. The rather scattered appearance of these results is to be expected in view of the low significance of the lowest isolevel contours (see again table 1).

The most striking characteristic of figures 17(*b–d*) and 18(*b–d*) is that the centre of the wake, approximately from $-l_0$ to $+l_0$, appears to be a well-stirred flow, because no organization departing from the conventional mean values and related to the large-scale motions is observed in the squared velocities or the second derivatives. In fact, this should not be a surprise as even in the velocity patterns, figures 17(*a*) and 18(*a*), it can be observed that the highest isolevel contours fail to cross the wake, the link between both sides of the wake being established by the 25% contour. In addition it can be seen that the contribution to the r.m.s. value (figures 17*b* and 18*b*) in the edges of the wake is always positive for the negative velocity fluctuations associated with the passage of the rollers, while the positive velocities in the trailing or leading edges of the double roller show a lesser contribution.

The ensemble averages of $\langle U^2\rangle - \langle U\rangle^2$, displaying the fluctuations of the family of patterns over its ensemble average, are presented in figures 17(*c*) and 18(*c*). Non-zero values are concentrated more than ever in the edges of the wake. High fluctuations are observed in the tops of these eddies which are consistent with the velocity patterns of figure 12. The outermost anemometer in the wake sometimes senses positive velocity fluctuations (figure 12*b*) but also on occasion near zero (figure 12*d*) or negative velocities (figures 17*a* and 18*a*), depending on the alignment of the anemometer with respect to the centre of the roller. Hence the fluctuations of the individual patterns with respect to their mean is high. Moreover, the trailing and leading edges of the double rollers made up of 'younger', newly entrained flow, show less variation than the mean r.m.s. values of the anemometers. The -10% isolevel contour in both figures 17(*c*) and 18(*c*) not only marks the youngest flow in the ensemble averge, but also expands towards the centre of the wake. This indicates that although most of the organized activity in the wake seems to be concentrated at the edges, the velocities averaged to obtain the ensemble of figure 17(*a*), and particularly of figure 18(*a*), show less variation among them than the conventional r.m.s. values at a significance level of 10% and 3.5%, respectively.

Finally the ensemble averages of the envelope of the second derivatives are plotted in figures 17(*d*) and 18(*d*). The behaviour of these is much the same as that observed for the ensembles of the squares of the fluctuating velocities, and so analogous comments can be made. Although the centre of the wake does not display coherent activity linked to the passage of double rollers, at the edges of the wake, from $\pm l_0$ outwards, it is clear that the fine-scale activity depends solely on the presence of these eddies. Thus they not only seem to be responsible for the entraining motions, but also for the transportation of old, turbulent flow from the centre of the wake towards its edges.

Apart from all the above points relating to the presentation of the ensemble averages of the squared velocities $\langle U^2\rangle$ and $\langle U^2\rangle - \langle U\rangle^2$ and of the second derivatives, there is a further aspect more related to the signal-processing side of the problem, that has to be highlighted. We argued that the $\langle U^2\rangle - \langle U\rangle^2$ ensemble averages should not be used to construct fine-scale activity maps because they represent fluctuations over the ensemble mean and there is no guarantee that differences among individuals in one family of turbulent organized motions should come from fine-scale effects. This point is illustrated by comparing the results in the horizontal and vertical planes. In the horizontal plane (see figures 3, 5, 6, 15 and 16)

the three quantities $\langle U^2 \rangle$, $\langle U^2 \rangle - \langle U \rangle^2$ and the second derivatives show a different behaviour, while in the vertical plane of the wake (see figures 17 and 18) they display much the same distribution, although that does not mean the same information. Hence, if the squared fluctuating velocities were taken as a measure of the finer-scale activity, in some cases we would obtain information that would be qualitatively right, while in others we would be definitely wrong in our understanding of the flow.

6. Final discussion

So far we have been presenting a series of results and several hypotheses on the large-scale organization and the fine-scale activity of the far wake which have been checked against the experimental findings. The question of whether most of these hypotheses are correct or are only part of the truth is one that requires more information than we have available before a definite answer can be given. In particular it would be extremely helpful to analyse $\times$-wire signals or simultaneous temperature and velocity signals since at present circulation has to be inferred only from u-velocities and the effect of the detected eddies on entrainment deduced from separate records of velocity and temperature. Nonetheless, despite the limitations of u-data, the hypothesis of the existence of the double-roller eddies in the far wake and, perhaps more important, their energy content and relation to the fine-scale activity, seems to be supported by other experimental evidence, and has even been used to explain some additional significant experimental observations.

What follows should be considered as a general discussion on the nature of turbulence dynamics in view of the results obtained. Some ideas that have been widespread in the turbulence literature and that have been checked mainly against time-averaged measurements, but seldom compared with instantaneous ensemble-averaged measurements, are reviewed. The first thing that is worth noting is the true three-dimensional character of the turbulence, which is so important that no understanding of any turbulent flow seems possible without taking it into account. The far-wake flow appears dominated by an organized motion which exhibits a very strong vorticity content in a direction different from the vorticity of the mean flow so that the latter appears, in fact, to be unrelated to the vorticity of the typical large-scale eddies. The homogeneity of the flow in the z-direction is guaranteed by the alternate sign of the vorticity in the two vortices that make a double-roller eddy and by their freedom to be aligned at any z-position. This is in fact what homogeneity means: the same statistical description of the flow will be attained independently of the z-coordinate of sampling in the flow. However, homogeneity does not mean more than this, and any further hypothesis on 'homogeneous' coordinates of the problem based on mean flow measurements which could be taken to analyse the dynamics of the instantaneous turbulent field, will lead to a misunderstanding of the true features of the turbulence.

The key to the problem is to understand the role played by the large-scale motions, in this case the double-roller eddies, in the turbulence activity. It appears that the rollers contain about 40% of the energy of the fluctuating field. Also, they seem to control the process of entrainment, which could be regarded as the beginning of the energy cascade that transfers energy from the mean flow to the fully turbulent centre of the wake. Moreover the fine-scale activity is observed to concentrate in the vortical cores of the double-roller eddies. In fact, if they contain 40% of the energy and are the structures that act as a source of energy, then the sink of the energy, i.e. the dissipative effects, could not occur in any other place unless the energy necessary

to sustain the smallest eddies were transmitted over a distance. Hence, it appears that the spotiness of the finer scales of the turbulence is not contradicted by the assumed isotropy of small eddies in a turbulent flow, because the concepts 'spotiness' and 'isotropy' correspond to two different domains.

If dissipation is understood to be a constraint of the turbulent energy budget, but not its driving mechanism (Laufer 1983), we would arrive at the conclusion that the finer scales of the turbulence can develop only over the large scales that effectively take energy from the mean flow, because if there is no input to the energy cascade it is not possible to dissipate energy. So then, it seems reasonable that the spots of fine-scale activity should appear at intervals of the order of the integral scales of the flow, because the latter are fixed by the large-scale motions within which we can imagine to be 'confined' the spots of dissipation. Isotropy in the fine scales can be related to the lack of preferred orientation of the smaller eddies, which would virtually lead to the isotropization of fine-scale fluctuations of the three components of the velocity.

The lack of preferred orientation can be explained as a consequence of the fact that the finer scales develop as secondary instabilities over the large-scale motions. If the large eddies are already filling one degree of freedom in the physical space, successive steps in a chain of secondary instabilities will randomly fill new degrees of freedom, in such a way that although the smaller eddies may always be the same kind of eddy, their effects would appear as fully random fluctuations. This 'internal' spotiness is not inconsistent with our findings, and in fact we believe that the reason why the ensemble averages of the second derivatives show such scatter and low peak values is that not all the individual realizations in one family of patterns show high values of the second derivatives in the same positions, even within the strong negative velocity lobe in the centre of the double roller.

If the mechanism described were appropriate to the energy cascade of the turbulence, it would appear that the conventional image of large eddies that split and split again to produce smaller eddies until they arrive at the scale dominated by the viscous dissipation is only one of the possible ways the energy transfer could be established. When a big eddy splits and becomes smaller it loses its direct interaction with the mean flow, and hence its ability to extract energy from it. Thus, a dissipative eddy would prefer, if possible, to grow over a large eddy that were in a situation of dynamical equilibrium gaining and loosing energy steadily, rather than participate in the decay cycle of a large-scale motion that is being annihilated. However, things cannot be so simple because the small eddies removing energy from a large structure to the dissipative scales are not only its own secondary instability eddies, but also small eddies captured or strained by the large-scale flow.

Dynamical equilibrium can also be understood in the sense that the structures are in equilibrium not because they are in some steady state, but because they are created and destroyed at the same rate. This highlights an idea that was part of the previous discussion, as well as included in much of the discussion related to the observation of the double-roller eddies at several downstream positions in the wake of a single cylinder and many other wakes (FG1). Particularly illuminating are the results on the evolution of the Kármán vortices from $x/D = 10$ to $x/D = 60$, and the detection of roller eddies from $x/D = 60$ to $x/D = 220$ in the wake of a single cylinder presented in FG1.

First, the Kármán vortex street was observed in FG1 to gradually lose its periodicity, mainly owing to a randomization effect produced by the annihilation of individual vortices as a result of the dissipative effects of the turbulence. At $x/D =$

60 only a few of the total number of vortices shed by the cylinder were detected, but as early as $x/D = 30$ (Ferré 1986) velocity patterns consistent with the presence in the flow of double-roller eddies could be observed. Therefore, the Kármán vortices shed from the cylinder may be regarded an example of large eddies that do split and split again, this transferring energy to the small scales. However, Kármán vortices are not able to regenerate in the wake because their generating mechanism resides in the instabilities of the boundary layer over the cylinder, which are not present in the flow itself. The Kármán vortices are in the near wake because they have been shed by the cylinder, but are a foreign flow organization that seems to be condemned to disappear essentially because they are not able to extract energy from the mean flow, even though their vorticity is aligned with the mean flow vorticity. Some of them can apparently survive these dissipative effects, as indicated by the fact that the strongest reduction in Kármán vortices occurs from $x/D = 10$ to $x/D = 30$, while from $x/d = 30$ to $x/D = 60$ the reduction is much lower. However, the ones that survive beyond $x/D = 60$ do not seem to play any special role in the far wake because the flow there behaves independently of initial conditions (FG1). The position where self-similarity is attained, however, differs between a normal wake and a wake where the shedding of Kármán vortices has been inhibited because the remains of the vortex street helps to attain self-similarity.

In comparison with the Kármán vortices, the double-roller eddies have been observed from $x/D = 60$ to $x/D = 220$ in the wake of a single cylinder and in several wakes at $x/D = 140$. Furthermore, Grant (1958) postulated their existence from correlation measurements made at more than five hundred cylinder diameters. From past and present experimental evidence, it seems reasonable to assume that double rollers evolve from spanwise vortex lines rotated and stretched by the action of shear, resulting in a horseshoe structure aligned with the mean rate of strain. Agreement between theoretical predictions and experimental measurements in both laminar and turbulent wakes (Wyganansky, Champagne & Marasli 1986; Cimbala, Nagib & Roshko 1988) points to the hydrodynamic instability of the mean velocity profile as the generating mechanism of such kind of spanwise vortex lines. Also, it has been observed by visualization (Cimbala *et al.* 1988) that even in a laminar wake these vortex lines are subject to secondary instabilities, leading to three-dimensional hairpin structures.

The enhancement of vorticity caused by stretching the legs of the horseshoe eddy increases backflow at the centre of the rollers, and, thus, the ω_z value of the top of the horseshoe and the rate of entrainment. The intense velocity gradients in a roller will in turn favour secondary instabilities that would increase the effective viscosity, until the double roller breaks into smaller eddies, terminating its interaction with the mean flow.

The formation of double rollers from vortex lines explains why they are detected with a preferred sense of rotation. The side of the wake towards which these vortex lines are pulled depends only on their sense of rotation with respect to the sign of mean shear. What is important to note is that this kind of reasoning can also justify why the entraining motions in a plane jet show a sense of rotation exactly inverted in sign with respect to the wake (Antonia *et al.* 1986): because the direction of the shear is inverted, the same kind of vortex line is pulled in the opposite direction than it would be in a wake.

Also consistent with the hypothesis that the double rollers are vortex lines stretched by the shear is that the plane of circulation of the vorticity in the legs of the rollers should be normal to the vorticity vector, and inclined with respect to the

vertical axis. This would provide the high correlation between the u- and v-components in the wake. But the $\overline{uv}$ term of the Reynolds stress is what brings the information from the fluctuating field to the time-averaged Navier–Stokes equations in the far wake and, thus, determines the mean velocity profile, which in turn provides the appropriate lengthscale for the self-preserving analysis of the wake. We therefore arrive at the conclusion that the wake becomes self-preserving as soon as it is able to forget its initial conditions and turbulence dynamics depend only on the mechanisms which take energy from the potential flow and dissipate it at the viscous scales. This point of view of the turbulent activity in the far wake could also explain why, despite the fact that the energy content of the flow may be reduced by an order of magnitude, the tendency to isotropization between the u-, v- and w-components of the velocity is fairly weak.

One assumption that has been used in the description of the generating mechanism of the double-roller eddies which has been taken for granted to be true, or at least appropriate, needs some further explanation. This is the idea that the vortex lines are rotated and stretched by the 'mean shear'. In fact, in the time-mean flow, vortex lines do not exist and the 'instantaneous' vortex lines in the wake are influenced by the 'instantaneous' shear, which could be quite different from the long-time-averaged 'mean' shear. However, the idea of a shear–vorticity interaction is not new. Indeed it is as old as the Navier–Stokes equations because when these are put in terms of vorticity and shear stress (Tennekes & Lumley 1972) they become

$$\frac{\partial \omega_i}{\partial t} + U_j \frac{\partial \omega_i}{\partial x_j} = \omega_j S_{ij} + \nu \frac{\partial^2 \omega_i}{\partial x_j \partial x_j}; \tag{15}$$

that is, the rate of change of the vorticity depends only on the viscous effects and on the shear stress–vorticity cross-product. Hence the shear will act to stretch the vorticity that is aligned with the eigenvectors of the S_{ij} matrix, and will rotate the other vorticity components.

What needs to be established is whether the eigenvectors of the instantaneous shear stress have more or less the same orientation as those of the mean shear. This is a problem quite different to just trying to evaluate the values of S_{ij} instantaneously, because matrices that appear quite different can have rather similar eigenvectors. To further pursue this line of thought, it has to be realized that what would be of more interest is not the instantaneous effects of the shear over vorticity, but its integrated action over the length of the vortex line, i.e. over a spatial region enclosing the volume of flow swept by the vortex line as its moves and evolves during the time interval in which the change of direction of the vorticity and vortex stretching takes place. This suggests that it is the 'short-time- and space-' averaged shear rather than the instantaneous shear that plays the main role. However, the experimental evidence we have obtained, points to very strong shear alignments in both the dynamic and thermal field. It therefore seems that the instantaneous shear has its eigenvectors effectively pointing in the same direction as the ones derived from the long-time-averaged mean shear. Obviously this is not a justification or a proof, but just a recognition that possibly our reasoning is correct.

We have discussed the evolution of the near Kármán vortex street stating that the Kármán vortices are not able to extract energy from the mean flow, and that their means of destruction is by the action of dissipative effects. However at $x/D = 60$ both Kármán vortices and double-roller eddies could be identified in the wake. Why is this so? Is it just that there were too many vortices in the wake? In some sense

we think that this is part of the answer. The turbulence intensity in the near and intermediate wake is so high, owing to the strong energy content of the Kármán vortices shed by the cylinder, that there is no effective short-time- and space-averaged shear sufficient to select Kármán vortices as if they were vortex lines in the far wake. Only as the turbulence intensity decays in the wake, and the short-time-averaged velocity profiles become more and more similar to the mean velocity profile do the described mechanisms begin to act.

It is possible to present some figures to give support, albeit rather indirectly, to the hypothesis that the short-time- and space-averaged shear could have eigenvectors close to the ones of the mean shear. The evidence is indirect because we will compare only short-time-averaged velocity profiles and the mean velocity profile. If U_{L} is the long-time average of a fluctuating velocity, and U_T is the short-time averaged velocity over a period T, then it can be shown that the variance of $U_T - U_{\mathrm{L}}$ depends on the integration time T, the turbulence intensity U_{RMS}, and the autocorrelation function of the fluctuating velocities R_{uu} (Tennekes & Lumley 1972), in such a way that

$$\mathrm{var}\,(U_T - U_{\mathrm{L}}) = \frac{2U_{\mathrm{RMS}}^2}{T}\int_0^T \left(1-\frac{t}{T}\right) R_{uu}(t)\,\mathrm{d}t. \tag{16}$$

If T is much longer than the integral scale of the turbulence, τ, then

$$\mathrm{var}\,(U_T - U_{\mathrm{L}}) = 2U_{\mathrm{RMS}}^2 \frac{\tau}{T}, \tag{17}$$

which is independent of the form of R_{uu}, and depends only on its integral, τ. However if T is just of the order of τ, a functional form for the autocorrelation function has to be assumed to solve the integral. Let us suppose that the autocorrelation can be approximated as $\exp(-t/\tau)$, then the variance of $(U_T - U_{\mathrm{L}})$ becomes

$$\mathrm{var}\,(U_T - U_{\mathrm{L}}) = \frac{2U_{\mathrm{RMS}}^2}{T/\tau}\left[\left(1-\frac{1}{T/\tau}\right)+\left(\frac{2}{T/\tau}-1\right)\exp(-T/\tau)\right]. \tag{18}$$

The typical length of the large eddies in a wake should be bigger than τ, since if the autocorrelation is of the form $\exp(-t/\tau)$ then for $t = \tau$ it is still as high as 0.37. Let us take a conservative value and evaluate the variance of $(U_T - U_{\mathrm{L}})$ for $T/\tau = 2$, then

$$\mathrm{var}\,(U_T - U_{\mathrm{L}}) = 0.50\ U_{\mathrm{RMS}}^2. \tag{19}$$

For plane wakes, an estimate of the turbulence intensities as a function of the maximum velocity defect in the wake, U_{M}, can be obtained (Tennekes & Lumley 1972) as

$$U_{\mathrm{RMS}} \approx 0.35 U_{\mathrm{M}}; \tag{20}$$

then, the estimate for the variance of $(U_T - U_{\mathrm{L}})$, or better, the expected r.m.s. value of the difference $(U_T - U_{\mathrm{L}})$ is

$$(U_T - U_{\mathrm{L}})_{\mathrm{RMS}} \approx 0.25 U_{\mathrm{M}}, \tag{21}$$

That is, the typical r.m.s. values of the short-time-averaged fluctuating velocities are of the order of 25% of the total velocity defect in the wake for an integrating time as short as two integral-scale units. These figures are only tentative because many other facts should be included in our analysis. However, they show that the

hypothesis regarding the short-time- and space-averaged shear stress was acceptable in the far wake.

The last aspect on which we would like to make some comments is the question of modelling turbulence in self-preserving wakes. The question is why is the simplest model with a constant turbulence viscosity (Tennekes & Lumley 1972) able to accurately predict the mean velocity profile at least when intermittency is taken into account in the edges of the wake? Why should such a simple model for the $\overline{uv}$ term of the Reynolds stress be appropriate? Tennekes & Lumley (1972) argue that this finding should not be taken to give support to any kind of 'mixing-length' theory, rather it has to be attributed to the simple fact that the flow is dominated by a single lengthscale. This is indeed true if the picture we have been presenting is correct. If the flow is characterized by a single type of motion or mechanism controlling the interaction between the turbulent flow and the mean flow then a single lengthscale may be sufficient. In other words we could say that there is only one way to transfer energy in the wake: by means of the double-roller/horseshoe eddies. There are other aspects of the model that are also in accordance with the experimental analysis, namely that the centre of the wake is a 'well-mixed' flow and that the differences at the edges of the wake can be attributed to intermittency, so that when this is taken into account the model still holds.

A final point concerns the form of the model itself, namely $-\overline{uv} = \nu_t \, \mathrm{d}U/\mathrm{d}y$. The correlation between u and v is taken to be proportional to the local mean shear $\mathrm{d}U/\mathrm{d}y$; this seems to be a reasonable assumption because the strength of the vortex stretching depends on $\mathrm{d}U/\mathrm{d}y$, and what maintains the correlation between u and v is the circulation in the legs of the double rollers, which is sustained in turn by the stretching effects of the shear on the vorticity of the double rollers.

This word has been financially supported by the CICYT, project PB85-0446, and the CIRIT.

REFERENCES

ANTONIA, R. A., BROWNE, L. W. B., BISSET, D. K. & FULACHIER, L. 1987 *J. Fluid Mech.* **184**, 423–444.

ANTONIA, R. A., CHAMBERS, A. J., BRITZ, D. & BROWNE, L. W. B. 1986 *J. Fluid Mech.* **172**, 211–229.

BROWNE, L. W. B., ANTONIA, R. A. & BISSET, D. K. 1986 *Phys. Fluids* **29**, 3612–3617.

CHEN, C.-T. 1979 *One-Dimensional Digital Signal Processing*. Marcel Dekker Inc.

CIMBALA, J. M., NAGIB, H. M. & ROSHKO, A. 1988 *J. Fluid Mech.* **190**, 265–298.

FABRIS, G. 1979 *J. Fluid Mech.* **94**, 673–709.

FERRÉ, J. A. Application of an artificial intelligence algorithm to the recognition of coherent structures in turbulent flows. 1986 Doctoral thesis, University of Barcelona (in Catalan).

FERRÉ, J. A. & GIRALT, F. 1989*a* *J. Fluid Mech.* **198**, 27–64 (referred to as FG1).

FERRÉ, J. A. & GIRALT, F. 1989*b* *J. Fluid Mech.* **198**, 65–78 (referred to as FG2).

FERRÉ, J. A., GIRALT, F. & ANTONIA, R. A. 1989 *Proc. 7th Symp. on Turbulent Shear Flows, Stanford, California, USA.*

GRANT, H. L. 1958 *J. Fluid Mech.* **4**, 149–190.

JIMENEZ, J., COGOLLOS, M. & BERNAL, L. P. 1985 *J. Fluid Mech.* **152**, 125–143.

LAUFER, J. 1983 *Trans. ASME* E: *J. Appl. Mech.* **50**, 1079–1085.

MUCK, K.-C. 1980 *Imperial College Aero Rep.* 80–03.

MÜLLER, U. R. & WU, J. 1987 *Proc. 6th Symp. on Turbulent Shear Flows, Toulouse, France*, 2.4.1–2.4.4.

MUMFORD, J. C. 1982 *J. Fluid Mech.* **118**, 241–268.

MUMFORD, J. C. 1983 *J. Fluid Mech.* **137**, 447–456.

PAYNE, F. R. & LUMLEY, J. L. 1967 *Phys. Fluids* **10**, S194–S196.

SAVILL, A. M. Effects on turbulence of curved or distorting mean flow. 1979 Ph.D. dissertation, University of Cambridge.

SREENIVASSAN, K. R. 1985 *J. Fluid Mech.* **151**, 81–103.

TENNEKES, H. & LUMLEY, J. L. 1972 *A First Course in Turbulence*. MIT Press.

TOWNSEND, A. A. 1956 *The Structure of Turbulent Shear Flow*, 1st edn. Cambridge University Press.

TOWNSEND, A. A. 1976 *The Structure of Turbulent Shear Flow*, 2nd edn. Cambridge University Press.

WYGNANSKY, I., CHAMPAGNE, F. & MARASLI, B. 1986 *J. Fluid Mech.* **168**, 31–71.